NASA Technical Memorandum 4050

Low-Speed Wind-Tunnel Test of a STOL Supersonic-Cruise Fighter Concept

Paul L. Coe, Jr., and Donald R. Riley

JULY 1988

NASA

NASA Technical Memorandum 4050

Low-Speed Wind-Tunnel Test of a STOL Supersonic-Cruise Fighter Concept

Paul L. Coe, Jr., and Donald R. Riley
Langley Research Center
Hampton, Virginia

National Aeronautics
and Space Administration

**Scientific and Technical
Information Division**

1988

Summary

A wind-tunnel investigation was conducted to examine the low-speed static stability and control characteristics of a 0.10-scale model of a STOL supersonic-cruise fighter concept. The concept, referred to as a twin-boom fighter, was designed as a STOL aircraft capable of efficient long-range supersonic cruise. The configuration name is derived from the long twin booms extending aft of the engine to the twin vertical tails, which support a high center horizontal tail. The configuration propulsion system features a two-dimensional thrust-vectoring exhaust nozzle which is located so that the nozzle hinge line is near the aircraft center of gravity. This arrangement is intended to allow large thrust-vector angles to be used to obtain significant values of powered lift while pitching-moment trim changes are minimized.

The results of the investigation indicated that the configuration exhibited significant nonlinear aerodynamic characteristics. Specifically, the results showed that the configuration exhibited a pitch-up tendency at an angle of attack of 8°. Deflection of the forward portion of the inboard wing panels (including the engine inlets) delayed the onset of pitch-up to an angle of attack of 10°.

Downward deflection of the jet exhaust nozzle (for thrust vectoring) produced additional circulation lift. Furthermore, with the horizontal tail off, thrust vectoring resulted in minimal changes in pitching moment.

Because of high levels of thrust-induced downwash, the horizontal tail was ineffective for providing longitudinal stability. Similar results were found for conditions with a revised horizontal tail repositioned to locations outboard of the aft tail booms. The horizontal tail remained effective for longitudinal control but was deficient in pitch trim capability. Finally, the configuration experienced a marked reduction in lateral and directional stability for angles of attack above 20°.

Introduction

A wind-tunnel investigation was conducted to examine the low-speed static stability and control characteristics of a 0.10-scale model of a STOL supersonic-cruise fighter concept. The concept, referred to as a twin-boom fighter, was designed as a STOL aircraft capable of efficient long-range supersonic cruise. The configuration name is derived from the long twin booms extending aft of the engine to the twin vertical tails, which support a high center horizontal tail. The propulsion system features a two-dimensional thrust-vectoring exhaust nozzle which is located so that the nozzle hinge line is near the aircraft center of gravity. This arrangement is intended to allow large thrust-vector angles to be used to obtain significant values of powered lift while pitching-moment trim changes are minimized. A complete description of the concept and design rationale is provided in reference 1.

The purpose of the present investigation was to obtain low-speed stability and control information over an angle-of-attack range including the stall. The investigation included a study of jet-induced power effects.

Symbols

Longitudinal forces and moments are referred to the wind-axis system and lateral-directional forces and moments are referred to the body-axis system. (See fig. 1.) The moment reference center is on the fuselage centerline and, unless otherwise indicated, is located longitudinally at 25 percent of the mean aerodynamic chord of the reference wing. This location is $0.118\bar{c}$ forward of the nozzle flap hinge line. The coefficients and symbols used are defined as follows.

b	wing span, ft
C_D	drag coefficient, Drag/qS
C_L	lift coefficient, Lift/qS
C_l	rolling-moment coefficient, Rolling moment/qSb
C_m	pitching-moment coefficient, Pitching moment/qS$\bar{c}$
C_n	yawing-moment coefficient, Yawing moment/qSb
C_T	thrust coefficient, Wind-off thrust force/qS
C_Y	side-force coefficient, Side force/qS
$\bar{c}$	mean aerodynamic chord of reference wing, ft (see fig. 2)
i_t	horizontal-tail incidence angle, deg
L_1	leading-edge segment of outboard wing panel (see fig. 2(b))
L_2	forward portion of inboard wing panel (see fig. 2(b))
q	free-stream dynamic pressure, lb/ft
S	planform area of reference wing, ft^2 (see fig. 2(b))
t_1, t_2, t_3	trailing-edge-flap segments of wing (inboard, mid, and outboard, respectively)
X, Y, Z	body reference axes (see fig. 1)

α	angle of attack of aircraft reference line, deg
β	angle of sideslip, deg
δ_a	aileron (segment t_3) deflection, deg
δ_e	elevator deflection, deg
δ_f	streamwise deflection angle of trailing-edge flap, deg
δ_{L_1}	deflection angle of leading-edge segment of outboard wing panel, deg
δ_{L_2}	deflection angle of forward portion of inboard wing panel, deg
δ_n	deflection angle of centerline nozzle, deg
δ_r	rudder deflection normal to hinge line, deg
ε	downwash angle, deg

Abbreviation:

c.g.	center of gravity

Derivatives:

$$C_{l_\beta} = \frac{\partial C_l}{\partial \beta} \qquad C_{n_\beta} = \frac{\partial C_n}{\partial \beta} \qquad C_{Y_\beta} = \frac{\partial C_Y}{\partial \beta}$$

Model

The investigation was conducted with the 0.10-scale model of a STOL supersonic-cruise fighter concept shown in figure 2(a). In addition to the baseline configuration, limited tests were also conducted to determine the effectiveness of the revised horizontal tail shown in figure 2(d). Jet power effects were simulated through use of model ejectors which were supplied by compressed air. Aerodynamic forces and moments were measured with a conventional six-component strain-gage balance that was mounted internal to the model. The model movable surfaces included the exhaust nozzle, wing leading- and trailing-edge flaps, twin rudders, and a single elevator. Surface deflections were obtained with preset angle brackets. All gaps were sealed for the test data presented.

Tunnel and Apparatus

The investigation was conducted in the Langley 12-Foot Low-Speed Tunnel. The model and internal strain-gage balance were mounted on a sting attached to a curved strut system so angle of attack could be varied. Sideslip angle was varied by rotation of the curved strut about a vertical axis. To ensure sufficient tail clearance, the model was located vertically above the centerline of the tunnel and was moved along an arc as angle of attack was varied. (See fig. 3.) Because the model was relatively small compared with the test section, no corrections have been applied to the data.

Tests

The tests were conducted at a free-stream velocity of 50.23 ft/sec (q = 3 psf), which corresponds to a Reynolds number of 0.58×10^6 based on the mean aerodynamic chord of the reference wing. Static-force tests were conducted over angles of attack from $-8°$ to $32°$ and angles of sideslip of $-5°$ and $5°$. Principal configuration variables included control-surface deflections and model thrust settings.

Presentation of Results

The results and discussion are presented as follows:

Results and Discussion

Longitudinal Aerodynamic Characteristics

Baseline configuration. Longitudinal aerodynamic characteristics for the baseline configuration with undeflected leading- and trailing-edge flaps and undeflected exhaust nozzle are presented in figure 4 for the horizontal tail off and on. As shown, for the tail-off configuration a mild pitch-up is observed near $\alpha = 8°$. This pitch-up typically results from lift generated on the forward portion of the wing by leading-edge vortices. If sufficient pitch control is available, artificial stability methods such as alpha feedback may be a means of stabilizing the configuration. In the present study, configuration modifications were

considered in an attempt to minimize or forestall this pitch-up tendency.

In figure 4 it is shown that for the horizontal-tail-on configuration the pitch-up characteristic is somewhat more pronounced than that for the corresponding tail-off configuration. As discussed in a subsequent section, for the conditions under consideration, this loss of horizontal-tail effectiveness for angles of attack greater than 8° is related to a significant nonlinear increase in the downwash angle ε, and thus an increase in $\partial\varepsilon/\partial\alpha$, at the horizontal-tail location. Similar variations of downwash angle with increasing angle of attack have been noted for T-tail aircraft configurations in which the high horizontal tail moves from a region of relatively slight downwash influence to a region of strong downwash influence with increasing angle of attack. The data of figure 4 also suggest that the basic airframe may experience a deep-stall stable trim point near $\alpha = 36°$.

Effect of deflection of wing leading edge. The results of deflecting the outboard-wing-panel leading-edge segment L_1 (see fig. 2(b)) of the present configuration are presented in figure 5. As shown, deflecting these particular leading-edge segments is ineffective in altering the nonlinearity of C_m. Inasmuch as the separated leading-edge vortex system is considered to originate well forward of the outboard-wing-panel leading edges, this result is expected.

In a further attempt to forestall the formation of separated wing leading-edge vortices, the entire forward portion of the inboard-wing-panel (segment L_2, see fig. 2(b)), including the engine inlet, was deflected downward. Figure 6 presents data for the baseline cruise wing with and without this forward inboard wing panel deflected 20°. As shown, deflection of the forward portion of the inboard wing panel delays the occurrence of pitch-up to $\alpha \approx 10°$ and delays wing stall. Figure 6 also shows that increasing the deflection to 30° results in no further improvement in the pitching-moment characteristics and results in degraded aerodynamic performance.

Trailing-edge effectiveness. Data for the effect of deflecting the exhaust nozzle from $\delta_n = 0°$ to $\delta_n = 42.15°$ (for the unpowered condition) are presented in figure 7. Also presented in figure 7 are data showing the effect of deflecting the wing trailing-edge flap in conjunction with the unpowered deflected exhaust nozzle. The data show that in this unpowered condition, deflecting the exhaust nozzle results in a slight positive increment in C_m. This result indicates that the center of pressure of the additional lift due to nozzle deflection is forward of the moment reference center. The incremental pitching moment produced by trailing-edge flap deflection indicates that for the conditions considered, the wing trailing-edge flaps begin to stall at angles of attack of about 16°. Unlike the exhaust nozzle, the wing trailing-edge flap hinge line is relatively far rearward of the moment reference center. Wing trailing-edge deflection results in an appreciable negative increment in pitching moment, and the stall of the trailing-edge flaps aggravates the previously discussed pitch-up tendency.

Effect of thrust. Wind-off static turning data for the configuration with an undeflected exhaust nozzle ($\delta_n = 0°$) and with a deflected exhaust nozzle ($\delta_n = 42.15°$) are presented in figure 8. Analysis of the data indicates that the thrust-vector angle is aligned with the exhaust nozzle deflection δ_n.

Figure 9 shows the effect of thrust on the static longitudinal aerodynamic characteristics of the configuration with $\delta_n = 0°$. Also presented in figure 9(a) are the computed values of C_L based on the relationship

$$C_L = C_L\Big|_{C_T=0} + C_T \sin\alpha$$

which assumes only a direct thrust contribution to lift. As shown, no appreciable additional circulation lift is produced and the lift and drag data show essentially the anticipated results. The data of figure 9(a) show very little effect of thrust on pitching moment, as would be expected because of the thrust vector passing through the moment reference center. However, for the configuration with the horizontal tail on (fig. 9(b)), the pitching-moment data show an unexpected positive increment associated with thrust. This result suggests the possibility of a thrust-induced loading brought about by downwash acting on the horizontal tail. To more clearly illustrate this thrust-induced downwash, the pitching-moment data of figure 9 are replotted in figure 10. As shown, thrust results in increasingly positive increments in the contribution of the horizontal tail to C_m.

Figure 11 shows the effect of thrust on the static longitudinal aerodynamic characteristics for the high-lift configuration with $\delta_n = 42.15°$ and $\delta_f = 20°$. Also presented in figure 11(a) are computed values of C_L based on the relationship

$$C_L = C_L\Big|_{C_T=0} + C_T \sin(\alpha + \delta_n)$$

which, as previously mentioned, assumes only a direct thrust contribution to lift. As shown, significant levels of additional circulation lift are produced for the configuration with $\delta_n = 42.15°$ and $\delta_f = 20°$.

Based on the theory presented in reference 2, the level of additional circulation lift achieved in the present tests is about 75 percent of the theoretical maximum. In figure 11(a) it is shown that, for the horizontal tail off, increasing thrust results in increasing negative increments in pitching-moment coefficient. For the horizontal tail on, the data of figure 11(b) indicate that at low angles of attack the magnitude of this thrust-induced negative increment in C_m is reduced, while at higher angles of attack it appears that thrust results in a positive increment in C_m. In order to isolate the direct-thrust effects from the preceding pitching-moment results, the data of figure 11 have been recomputed for a moment reference center corresponding to the exhaust nozzle hinge line ($0.368\bar{c}$) and are presented in figure 12. As shown in figure 12(a) (horizontal tail off), for angles of attack less than about $\alpha = 16°$ thrust has only a minimal effect on C_m, as expected. However, for the horizontal tail on, the data of figure 12(b) show that thrust produces a positive increment in C_m. In order to illustrate this point more clearly, the pitching-moment data of figure 12 are replotted in figure 13. As shown in figure 13, thrust results in a positive increment in the horizontal-tail contribution to C_m. This result is undoubtedly associated with a thrust-induced downwash, which produces a downward load on the horizontal tail. It should be further noted that for $\alpha \leq 8°$, thrust reduces the horizontal-tail contribution to static longitudinal stability. Although no downwash measurements were made, the reduction in horizontal-tail contribution to longitudinal stability is thought to be related to a thrust-induced increase in the downwash factor $\partial\varepsilon/\partial\alpha$.

Elevator effectiveness. Data showing elevator effectiveness for $\delta_n = 0°$ and $\delta_f = 0°$ and for $\delta_n = 42.15°$ and $\delta_f = 20°$ are presented in figures 14 and 15, respectively. As shown in figure 14, for the undeflected exhaust nozzle ($\delta_n = 0°$) the elevator effectiveness remains fairly constant over the test range of angles of attack and is not significantly affected by thrust. The data demonstrate that for the conditions under consideration, the horizontal tail and elevator are not stalled except for elevator deflection angles δ_e of magnitudes greater than about 20°. In the high-lift configuration with $\delta_n = 42.15°$ and $\delta_f = 20°$ (fig. 15), the data show that for the unpowered condition ($C_T = 0$) the elevator effectiveness is similar to the data for the cruise configuration (see fig. 14). For the power-on conditions ($C_T = 0.97$ and $C_T = 2.02$), however, it appears that the horizontal tail stalls for $\delta_e = -20°$. This result is probably related to the high levels of downwash which, as previously discussed, are associated with thrust vectoring.

Longitudinal trim. Examination of the data of figure 15 shows that the configuration is only slightly stable over angles of attack of $-8° < \alpha < 8°$ for $\delta_e = 0°$. The data of figure 15 also show that for $\alpha > 8°$ or for $\delta_e \neq 0°$, the configuration is longitudinally unstable. It is of course recognized that active controls in the form of alpha feedback to the horizontal tail may be a possible means for providing longitudinal stability, provided sufficient control power is available.

Figure 16 presents the regions of α vs C_T and C_L vs C_T for which (based on the data of fig. 15) sufficient longitudinal control exists to achieve $C_m = 0$. It is of course recognized that a comprehensive analysis including other pitch control requirements and static margin requirements would be necessary to determine if, in fact, unstable trim can be achieved for the regions presented in figure 16. However, the results summarized in figure 16 do serve to illustrate that the configuration is deficient in pitch trim capability.

Revised horizontal tail. As noted previously, for the high-lift configuration with $\delta_f = 20°$ and $\delta_n = 42.15°$, the high center tail is subject to a substantial thrust-induced downwash which results in the stall of the horizontal tail for $\delta_e = -20°$ and in a reduction in the horizontal-tail contribution to longitudinal stability. In an attempt to alleviate this condition, an alternate low outboard tail was considered. (See fig. 2(d) for geometric details.) The effects of thrust for this high-lift configuration with the modified horizontal tail off and on are presented in figure 17 for a design center-of-gravity location of $0.25\bar{c}$ and in figure 18 for a center of gravity coincident with the exhaust nozzle hinge line located at $0.368\bar{c}$. As discussed previously, this latter center of gravity was chosen in order to eliminate the direct-thrust-vector component from the pitching-moment coefficient. The pitching-moment data of figure 17 show increasing thrust results in significant negative pitching moments for the revised outboard tail configuration with a moment reference center of gravity located at $0.25\bar{c}$. However, the data of figure 18 indicate that the low outboard tail location is subject to a downward load as was the high center tail, and hence a high level of thrust-induced downwash also exists for the outboard tail location.

Control effectiveness for the all-moving revised horizontal tail is presented in figure 19. Analysis of the data of figure 19 shows that for the unpowered condition, the horizontal-tail downwash factor $\partial\varepsilon/\partial\alpha$ increases from about 0.5 for $\alpha < 4°$ to about 1.0 for $4 < \alpha < 16$. Therefore, as shown, the revised horizontal tail does not contribute to longitudinal

stability for $\alpha > 4°$. Furthermore, the revised horizontal tail does not alleviate the previously mentioned deficiency in pitch-trim capability.

From the preceding results it is apparent that to utilize the high-lift capability afforded by the thrust-vectoring system, an increase in horizontal-tail control power is required for pitch trim. One possible configuration would include both the high center tail (to maintain the structural advantage of the center tail section) in combination with the low outboard tail panels. Analysis of the data, with the assumption that the incremental results for the high center horizontal tail are linearly additive to those for the low outboard horizontal tail, results in the longitudinal control effectiveness depicted in figure 20. As shown in figure 20, this assumed configuration is unstable; however, the region for which unstable trim could be achieved by horizontal-tail alpha feedback is greatly expanded. It is of course recognized that other alternatives exist. One such alternative is to develop a high-lift horizontal tail mounted atop vertical tails of increased height. The increase in vertical-tail height could position the horizontal tail in a more favorable downwash field and thereby achieve both longitudinal stability and control.

Lateral-Directional Aerodynamic Characteristics

Static lateral-directional stability characteristics. Static lateral-directional stability characteristics were determined for $\beta = \pm 5°$ for the complete configuration with $\delta_f = 20°$ and $\delta_n = 42.15°$ and are presented in figure 21. The effective dihedral derivative C_{l_β} typically provides an accurate appraisal of the wing flow conditions. For the unpowered configuration, the occurrence of vortex separation at $\alpha \approx 4°$ is characterized by the nonlinear break in C_{l_β} data; the breakdown of the vortex core on the advancing side of the sideslipped wing apparently begins at $\alpha \approx 17°$ and is characterized by the break and subsequent positive slope of C_{l_β}; finally, the breakdown of both vortex cores apparently occurs at $\alpha \approx 25°$ and is characterized by the second reversal in C_{l_β}. Of course, the vertical tail also contributes to the effective dihedral. For the conditions considered, the reduction in C_{Y_β} with increasing angles of attack indicates that the vertical-tail contribution to C_{l_β} decreases with increasing angles of attack.

The directional stability derivative C_{n_β} is stable up to $\alpha = 22°$ but shows a marked reduction as α increases from 6° to 20° for $C_T = 0$. This condition is typically related to the progressive immersion of the vertical tails in the reduced-dynamic-pressure wake of the wing or the occurrence of adverse sidewash or both. As expected, based on the previous discussion of horizontal-tail effectiveness, power effects appear to increase the flow over the vertical-tail surfaces. For the power-on conditions investigated, the level of directional stability remains constant for $-8° < \alpha < 20°$. Above $\alpha = 20°$, a marked reduction in C_{n_β} is noted, and instability occurs at $\alpha = 24°$.

Rudder effectiveness. Rudder effectiveness is determined from data for $\delta_r = \pm 23°$ and is presented in figure 22. Based on the preceding discussion of directional stability, the variation of $C_{n_{\delta_r}}$ with α is expected. For the unpowered configuration there is a degradation in rudder effectiveness with increasing α; again, this degradation is thought to be due to the progressive immersion of the rudder in the wake of the wing. Power effects apparently provide an increase in flow over the tail surfaces which, in addition to increasing C_{n_β}, results in increased levels of $C_{n_{\delta_r}}$ up to $\alpha \approx 20°$.

Aileron effectiveness. Aileron effectiveness is determined from data for $\delta_a = \pm 20°$ and is presented in figure 23. These data were obtained for the cruise configuration (i.e., flaps and nozzle undeflected). The data show that for the conditions investigated the aileron effectiveness is maximum for $\alpha = 0°$ and the aileron effectiveness is significantly reduced as the angle of attack is increased to the point at which leading-edge separation occurs.

Summary of Results

A wind-tunnel investigation was conducted in the Langley 12-Foot Low-Speed Tunnel to examine the low-speed static stability and control characteristics of a 0.10-scale model of a STOL supersonic-cruise fighter concept. The results of the investigation indicate that the configuration exhibits significant nonlinear aerodynamic characteristics. Specific results are summarized as follows:

1. The configuration exhibited a pitch-up tendency at an angle of attack α of 8°.
2. Deflection of the forward portion of the inboard wing panels (including the engine inlets) delayed the onset of the pitch-up to $\alpha = 10°$.
3. Downward deflection of the jet exhaust nozzle for thrust vectoring produced additional circulation lift.
4. For the horizontal tail off, thrust vectoring resulted in minimal changes in pitching moment.

5. Significant levels of thrust-induced downwash acted on the horizontal tail.

6. The horizontal tail remained effective for longitudinal control but was ineffective for providing longitudinal stability and was deficient in pitch-trim capability.

7. The configuration experienced a marked reduction in lateral and directional stability for $\alpha > 20°$.

NASA Langley Research Center
Hampton, Virginia 23665-5225
May 27, 1988

References

1. Dollyhigh, Samuel M.; Foss, Willard E., Jr.; Morris, Shelby J., Jr.; Walkley, Kenneth B.; Swanson, E. E.; and Robins, A. Warner: *Development and Analysis of a STOL Supersonic Cruise Fighter Concept.* NASA TM-85777, 1984.
2. McCormick, Barnes W., Jr.: *Aerodynamics of V/STOL Flight.* Academic Press, Inc., 1967.

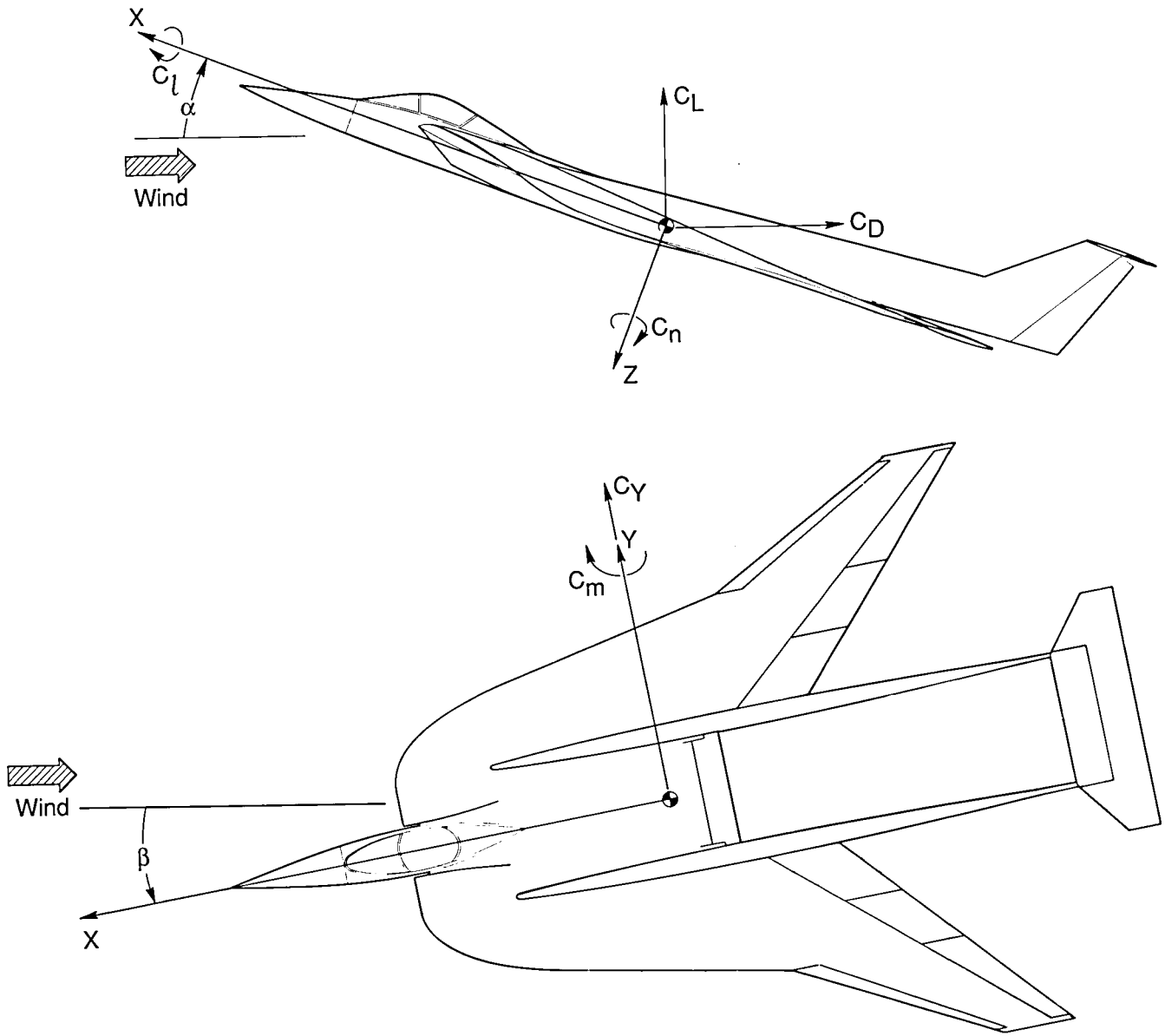

Figure 1. System of axes and angular notation.

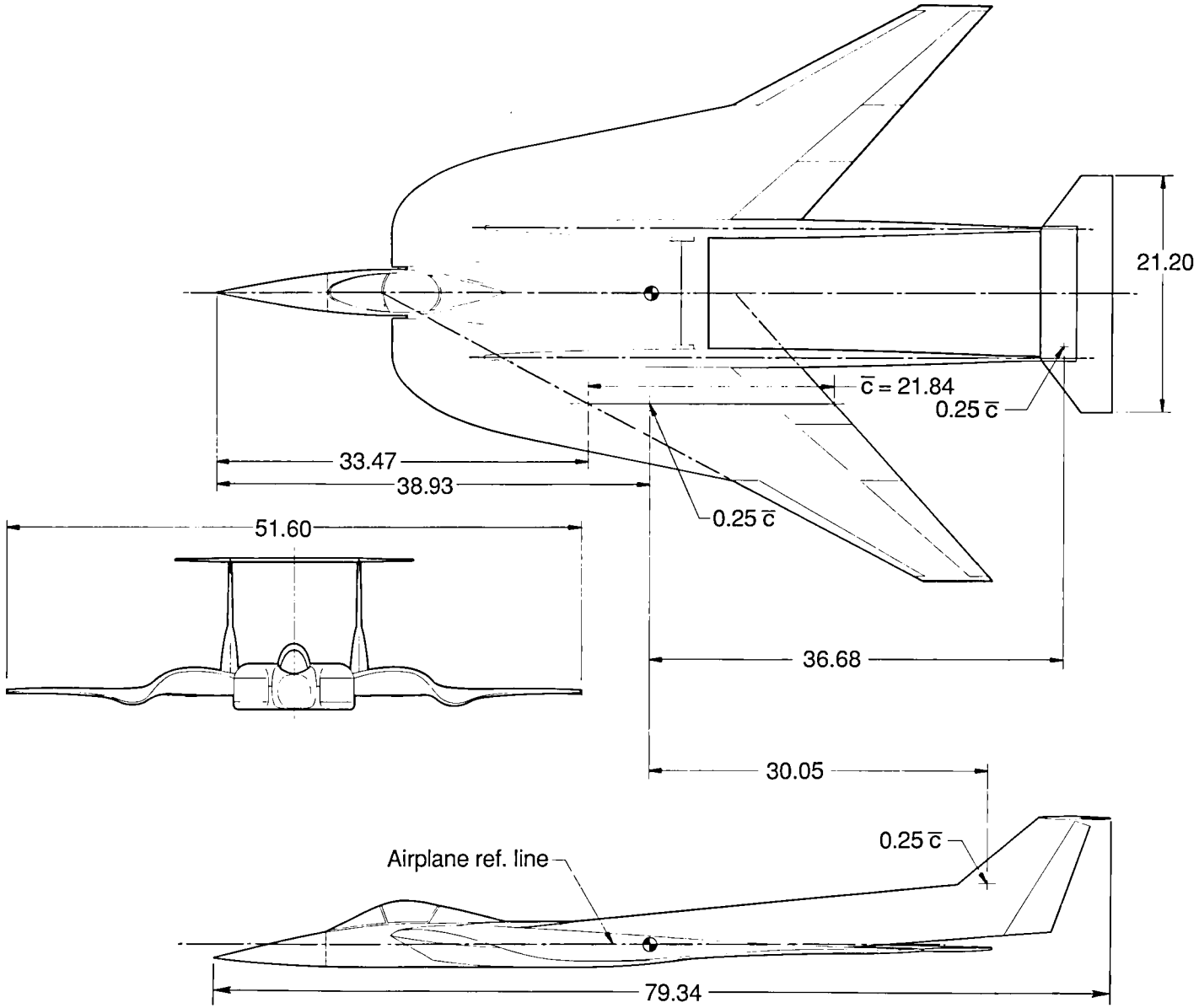

(a) Three-view sketch of baseline model.

Figure 2. Geometric characteristics of model. Linear dimensions are in inches.

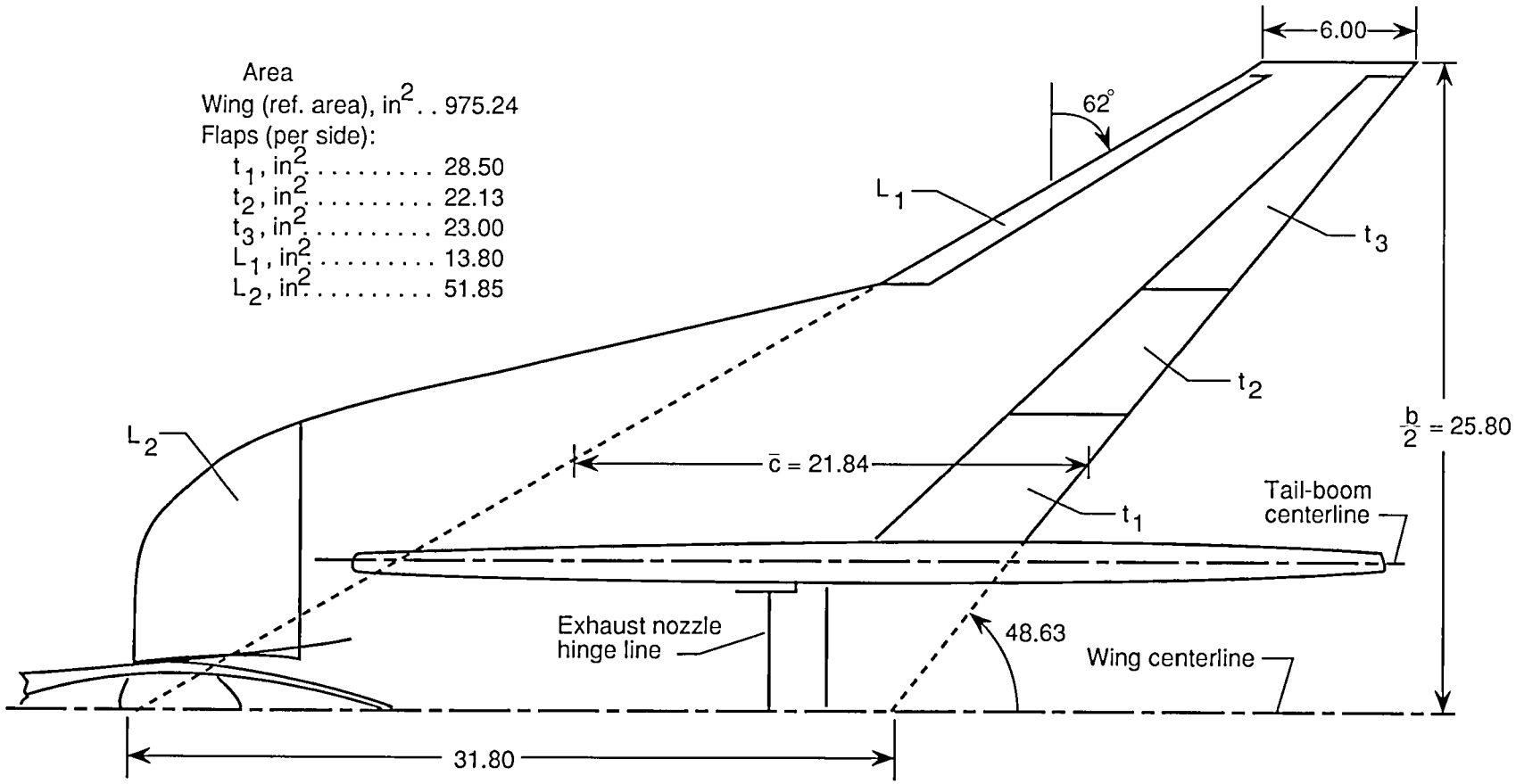

(b) Details of baseline wing.

Figure 2. Continued.

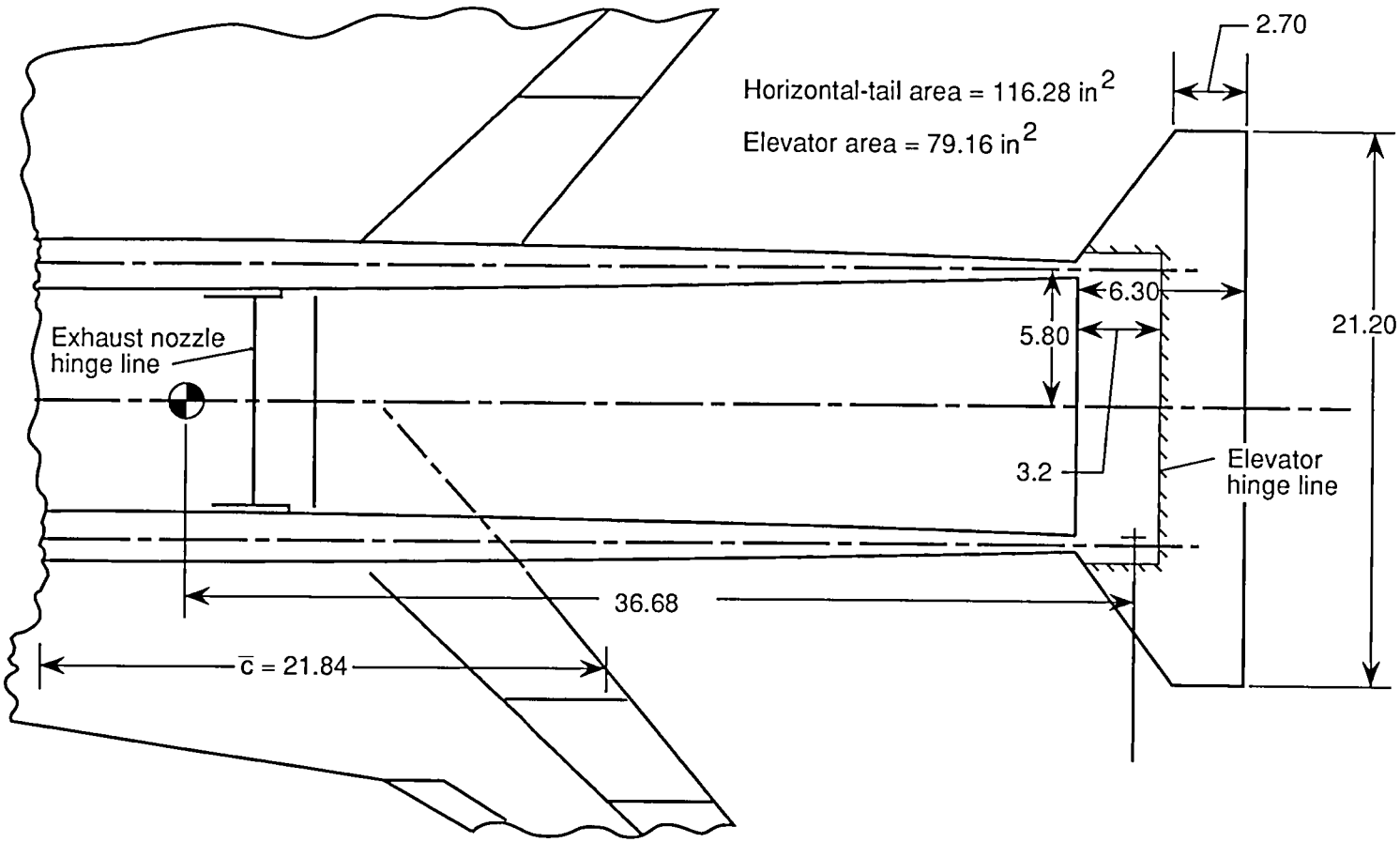

(c) Details of baseline horizontal tail.

Figure 2. Continued.

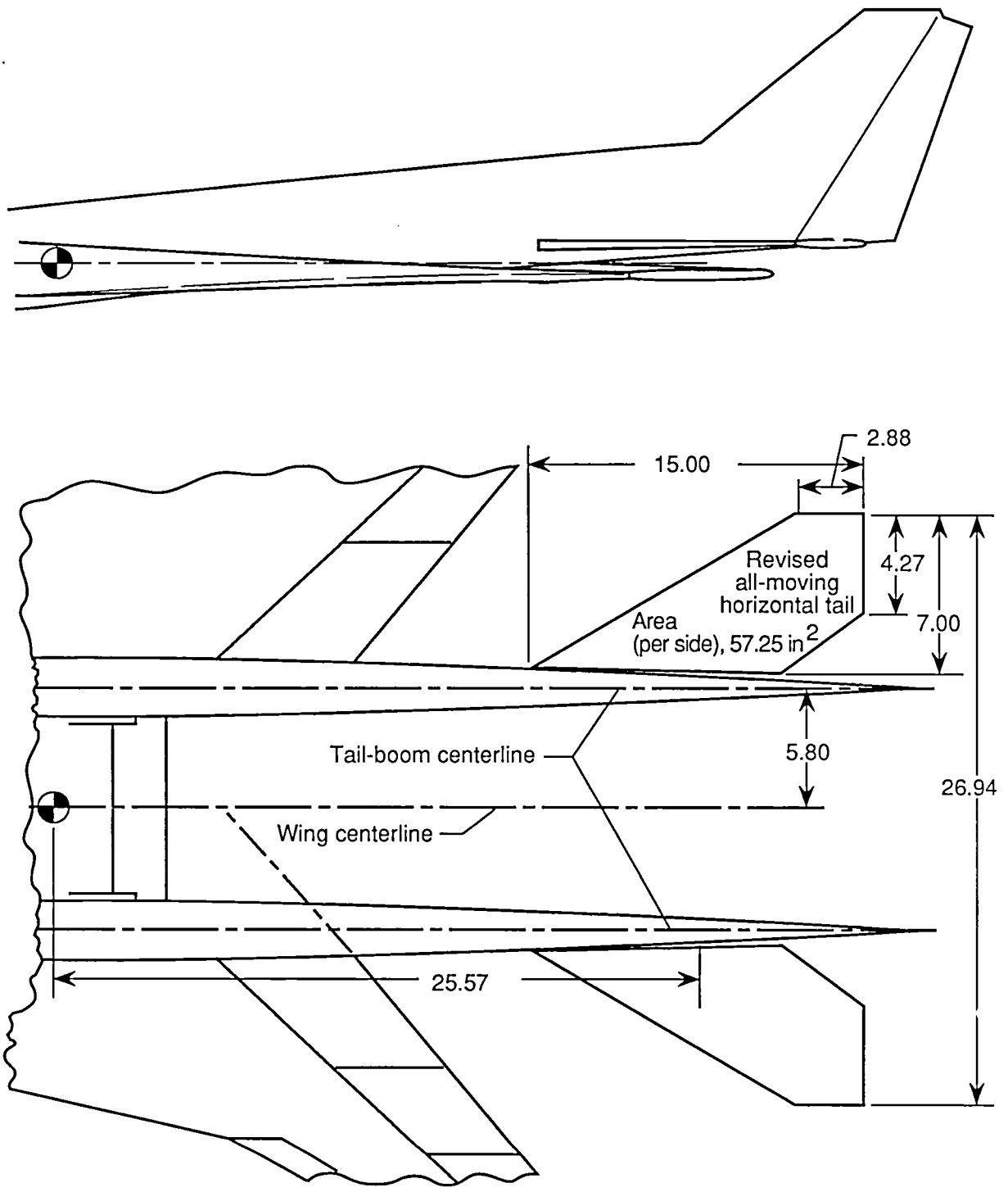

(d) Details of revised horizontal tail.

Figure 2. Concluded.

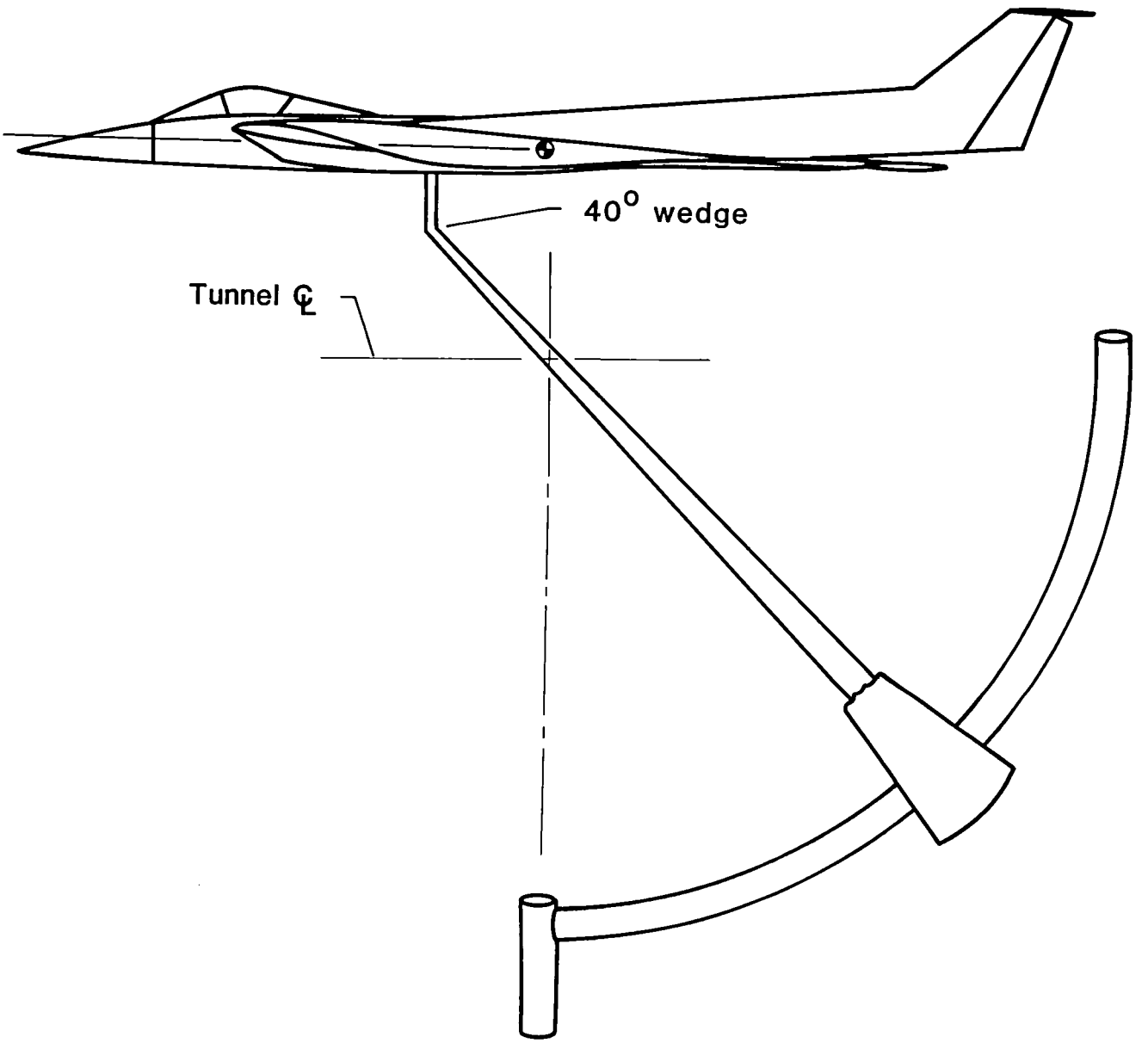

Figure 3. Model and support system as mounted in wind tunnel.

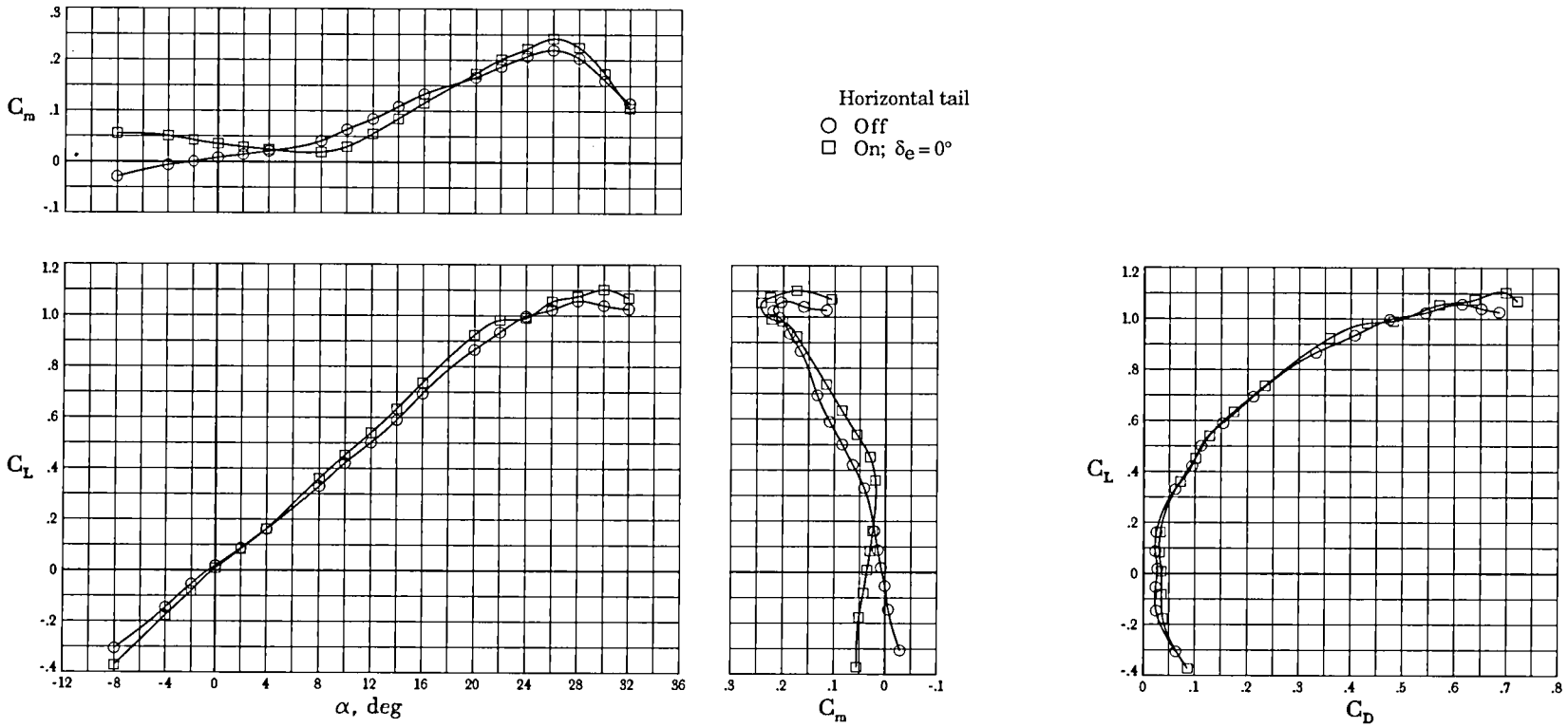

Figure 4. Longitudinal aerodynamic characteristics of baseline configuration. $\delta_{L_1} = 0°$; $\delta_{L_2} = 0°$; $\delta_f = 0°$; $\delta_n = 0°$; $C_T = 0$; c.g. at $0.25\bar{c}$.

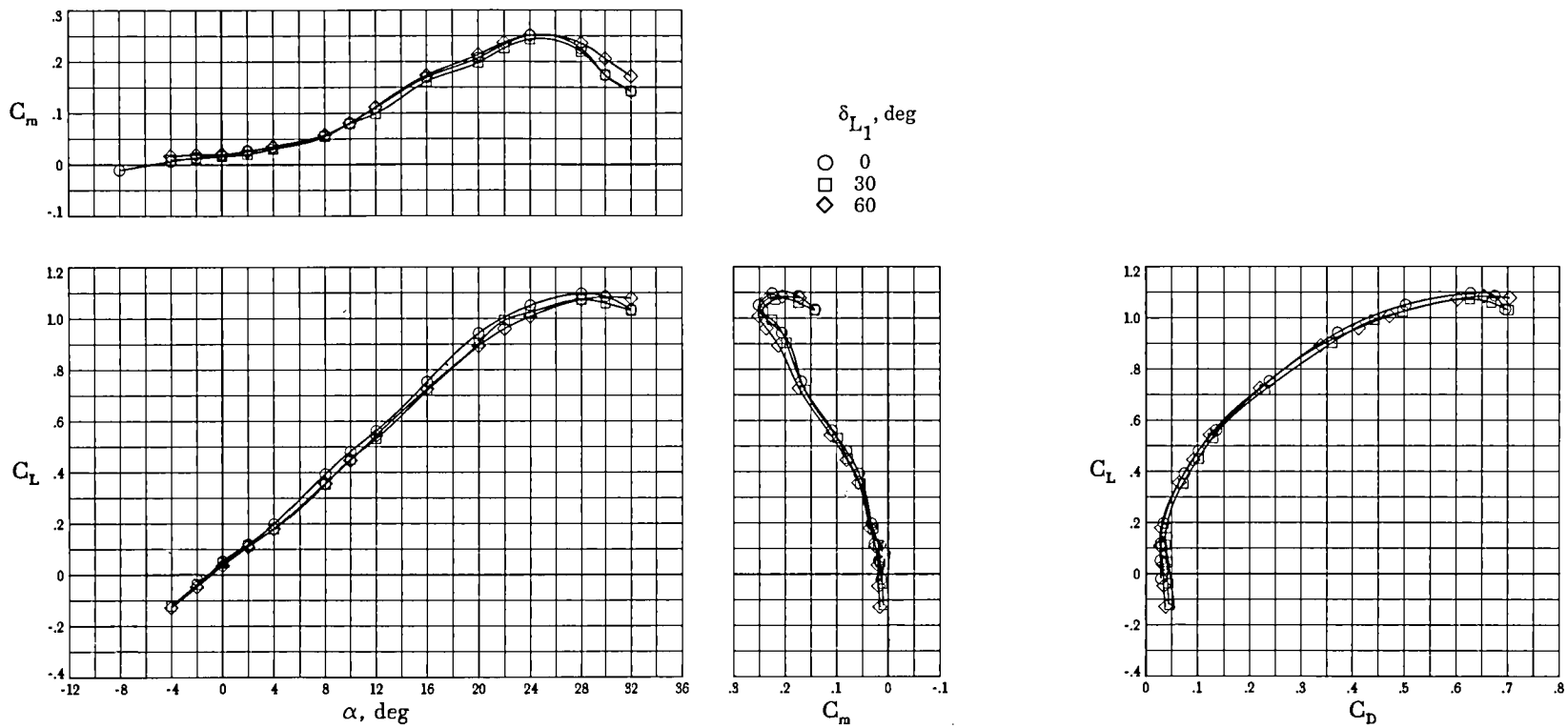

Figure 5. Effect of deflection of outboard-wing-panel leading edge. Horizontal tail off; c.g. at $0.25\bar{c}$; $\delta_{L_2} = 0°$; $\delta_f = 0°$; $\delta_n = 0°$; $C_T = 0$.

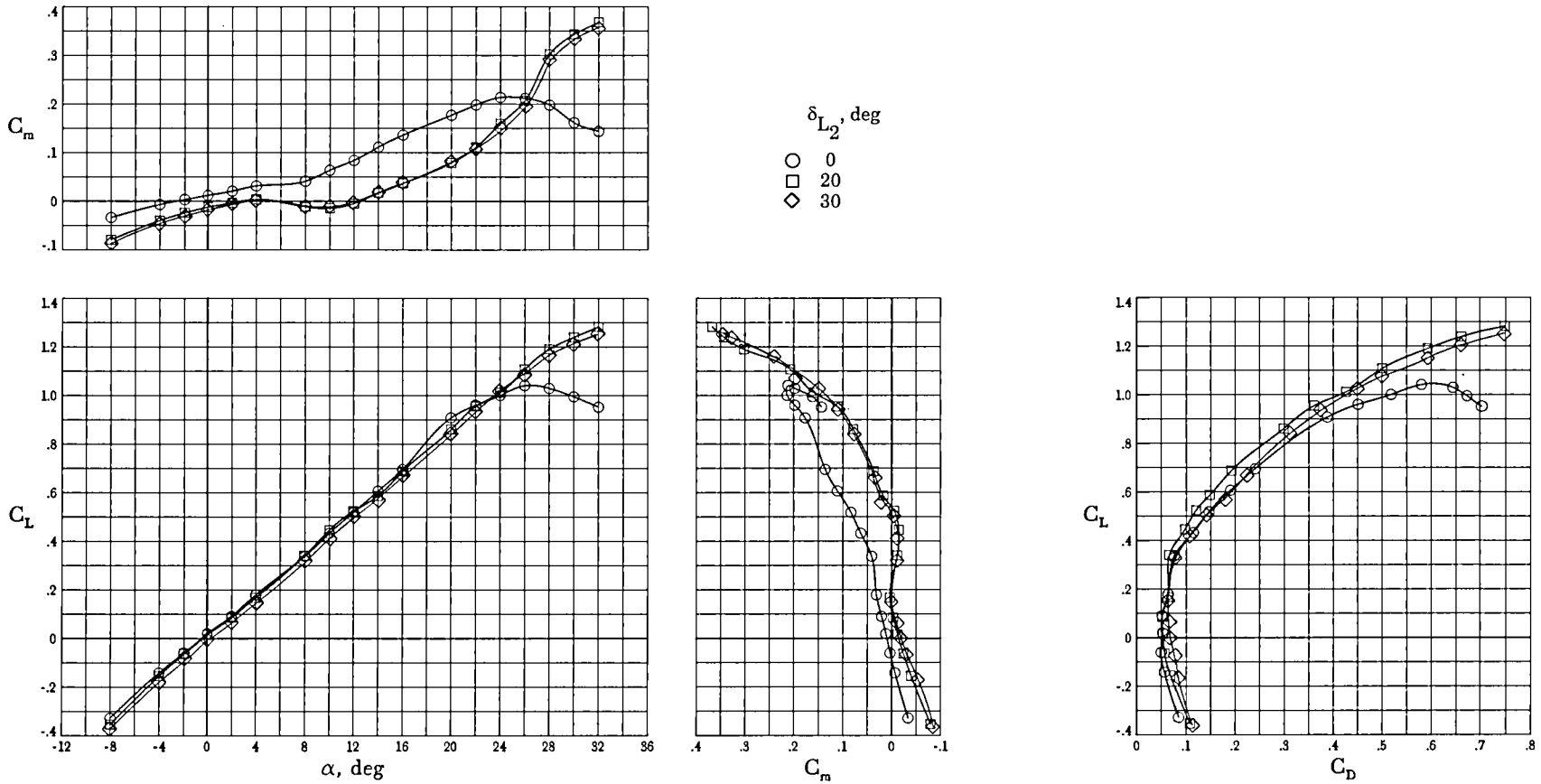

Figure 6. Effect of deflection of forward portion of inboard wing panel. Horizontal tail off; c.g. at $0.25\bar{c}$; $\delta_{L_1} = 0°$; $\delta_f = 0°$; $\delta_n = 0°$; $C_T = 0$.

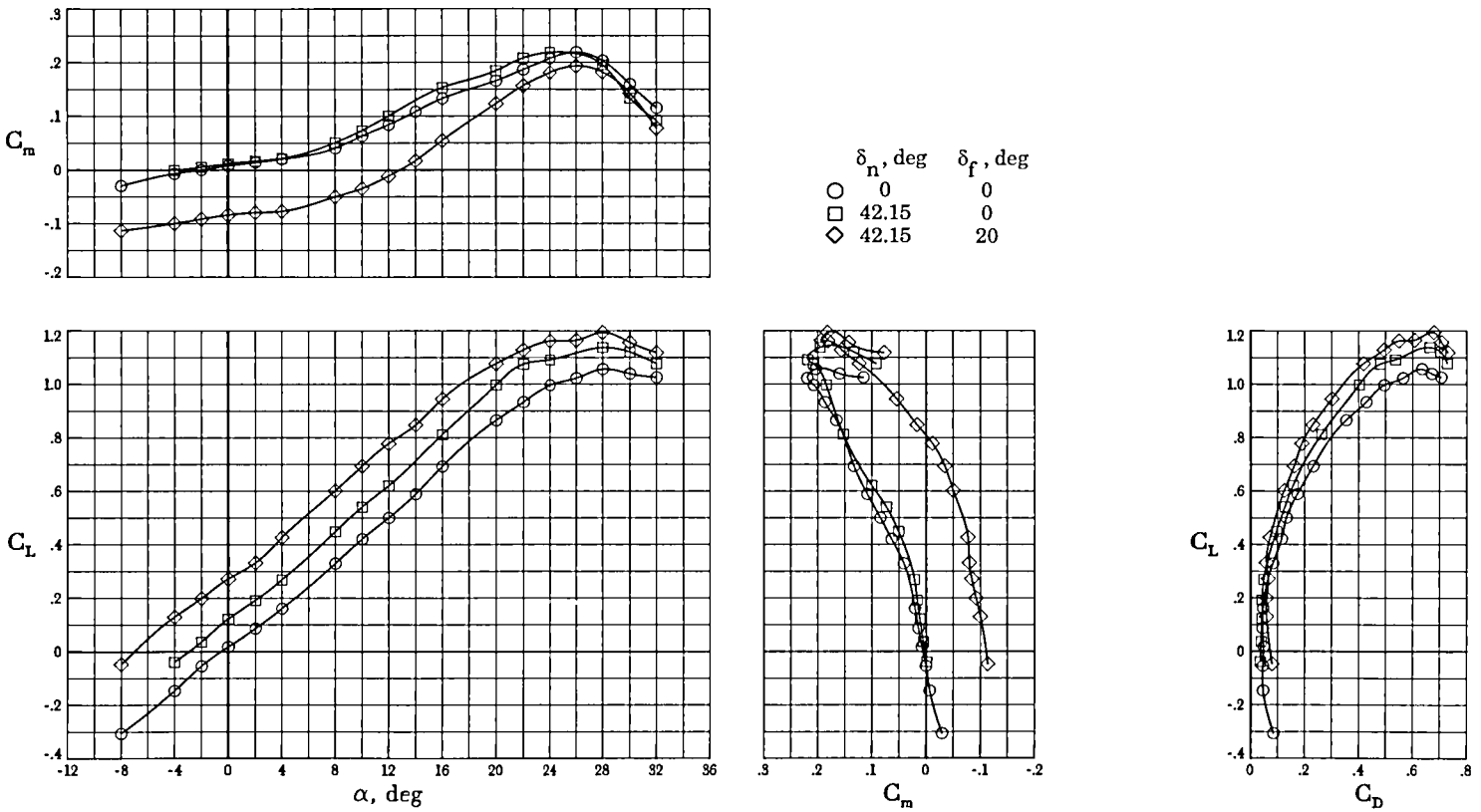

Figure 7. Effect of trailing-edge deflection. Horizontal tail off; c.g. at $0.25\bar{c}$; $\delta_{L_1} = 0°$; $\delta_{L_2} = 0°$; $C_T = 0$.

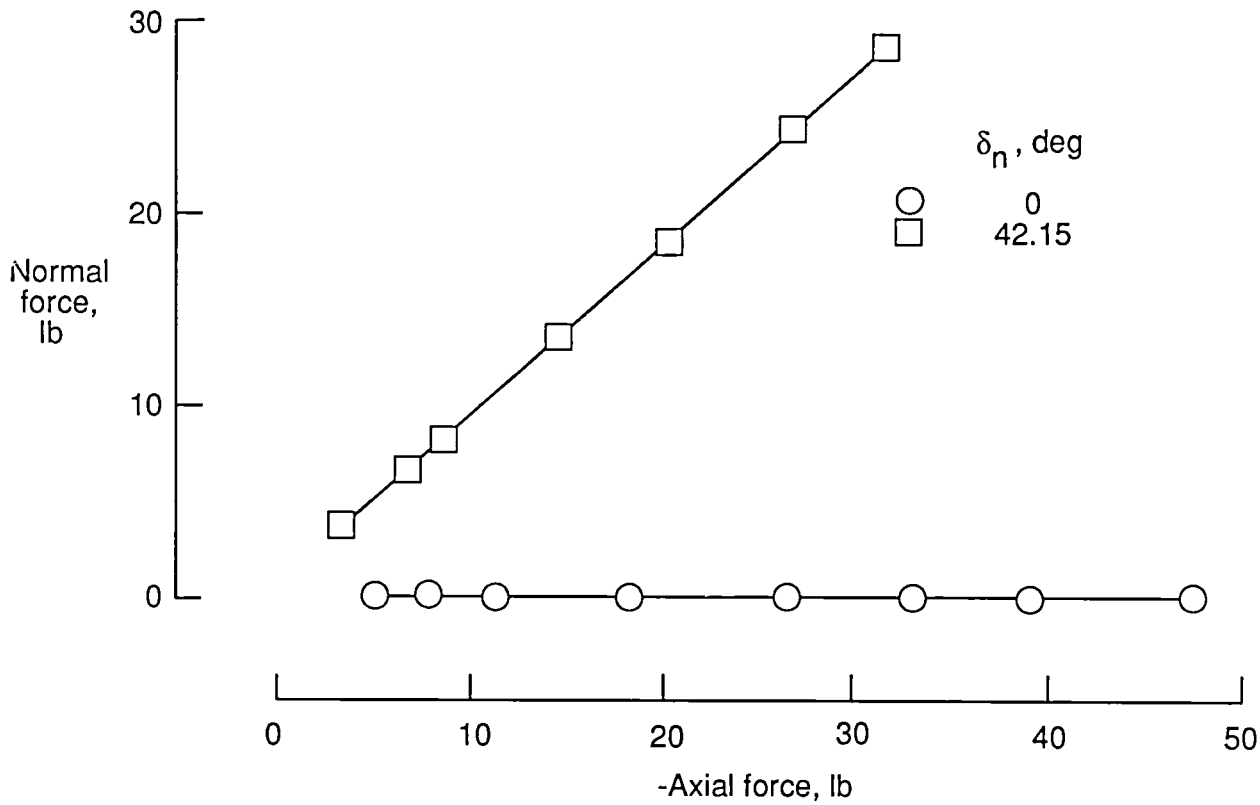

Figure 8. Results from static turning tests.

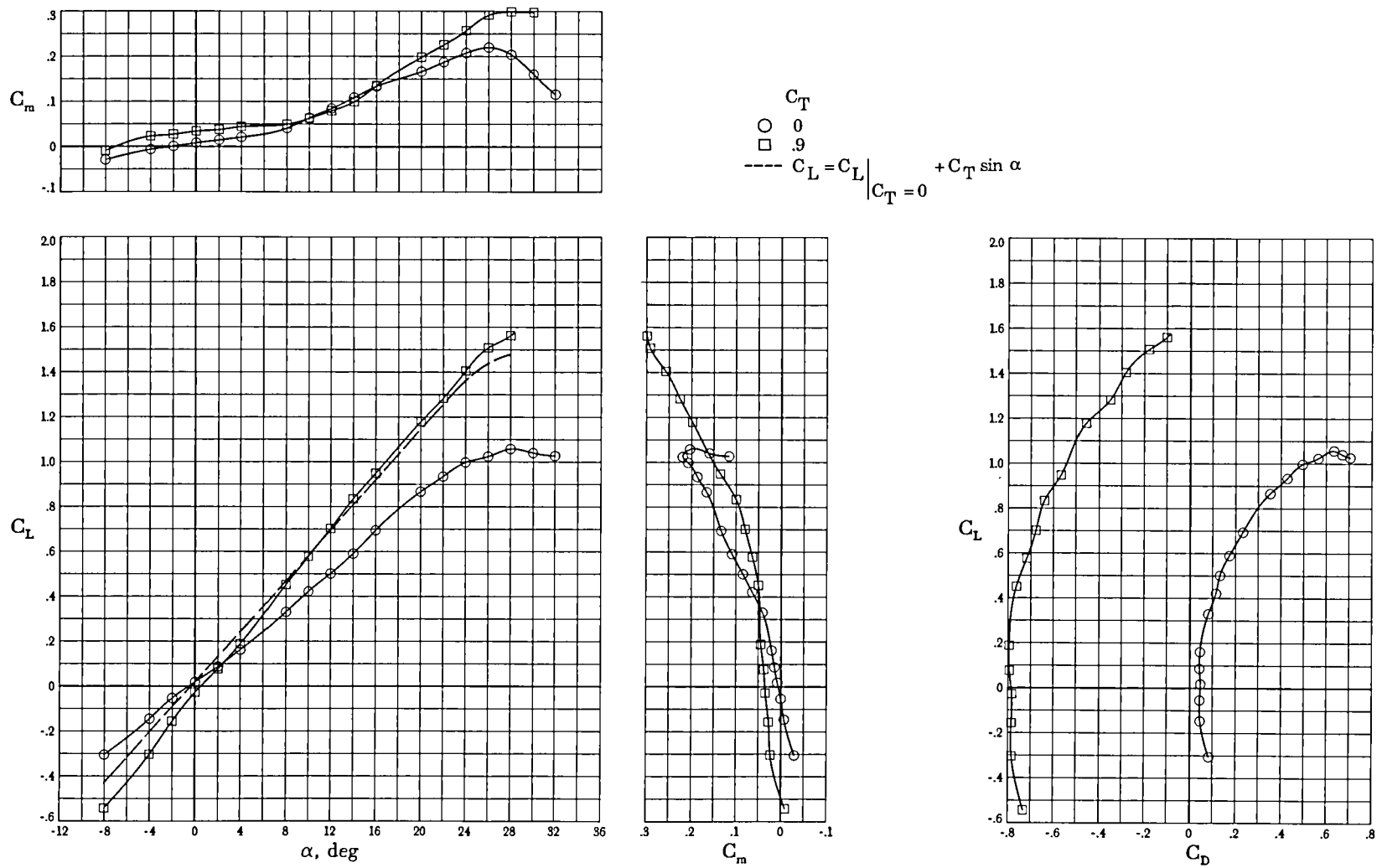

(a) Horizontal tail off.

Figure 9. Effect of thrust on longitudinal aerodynamic characteristics with $\delta_n = 0°$. $\delta_{L_1} = 0°$; $\delta_{L_2} = 0°$; $\delta_f = 0°$; c.g. at $0.25\bar{c}$.

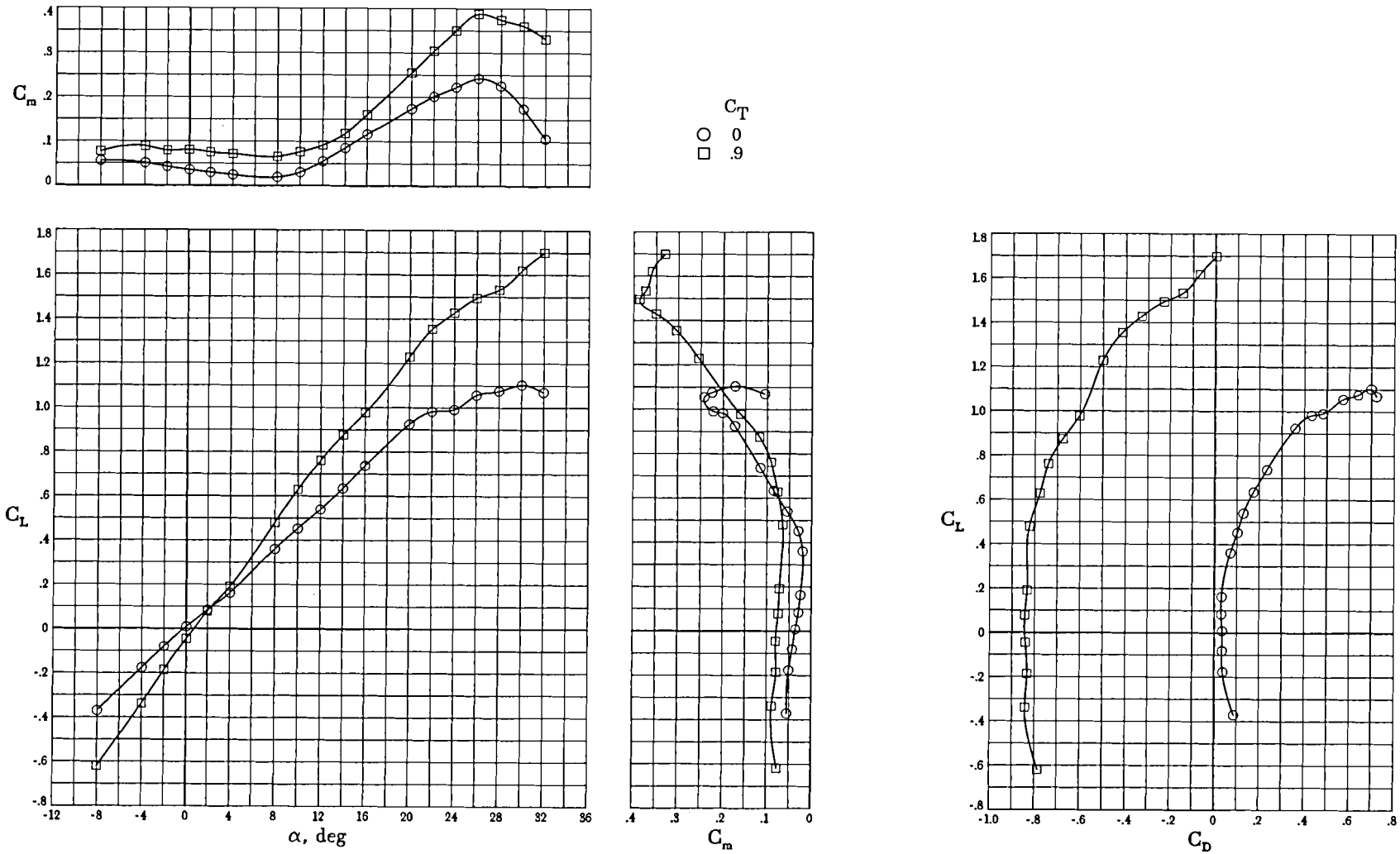

(b) Horizontal tail on; $\delta_e = 0°$.

Figure 9. Concluded.

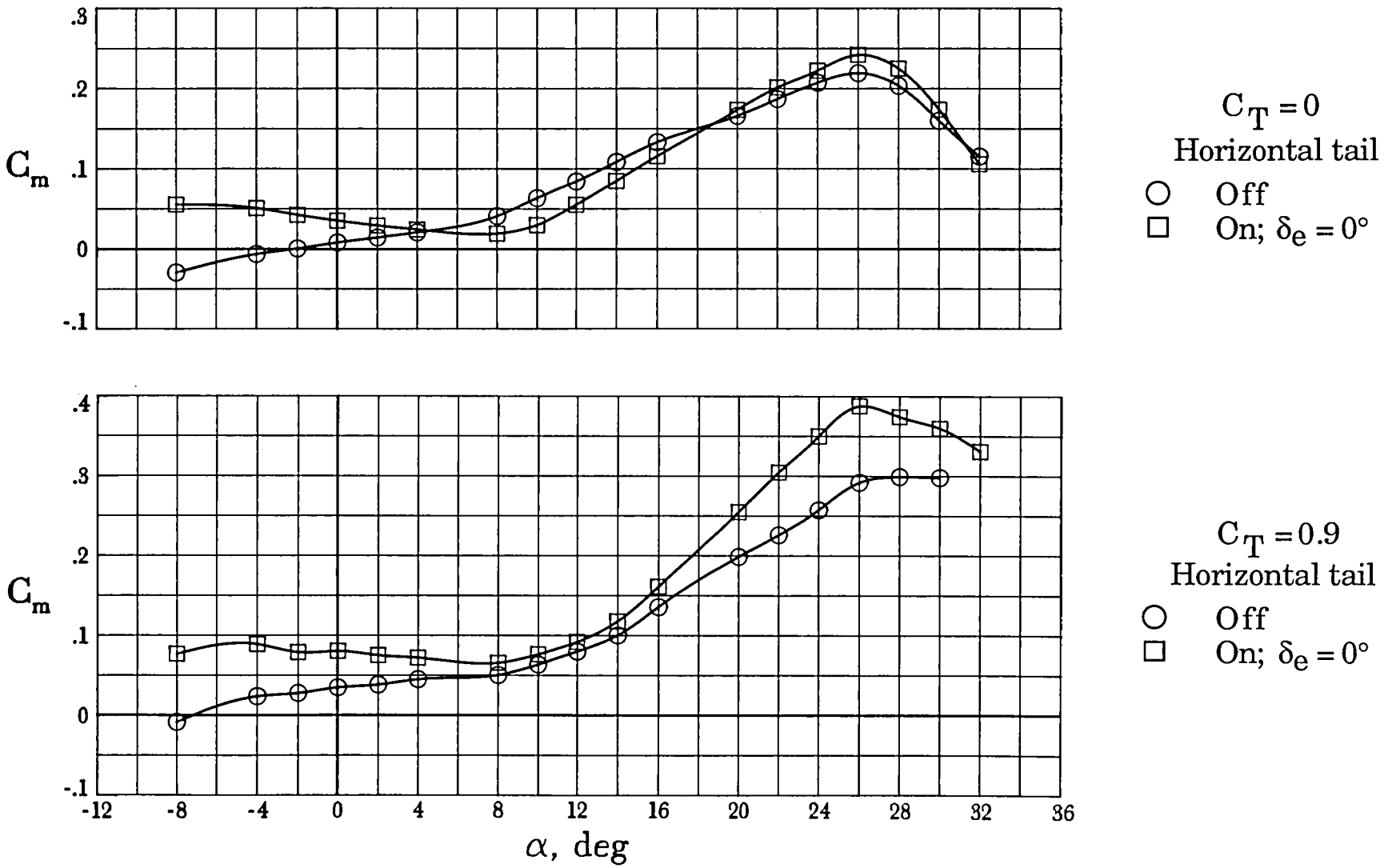

Figure 10. Effect of thrust on horizontal-tail contribution to C_m with $\delta_n = 0°$. $\delta_{L_1} = 0°$; $\delta_{L_2} = 0°$; $\delta_f = 0°$; c.g. at $0.25\bar{c}$.

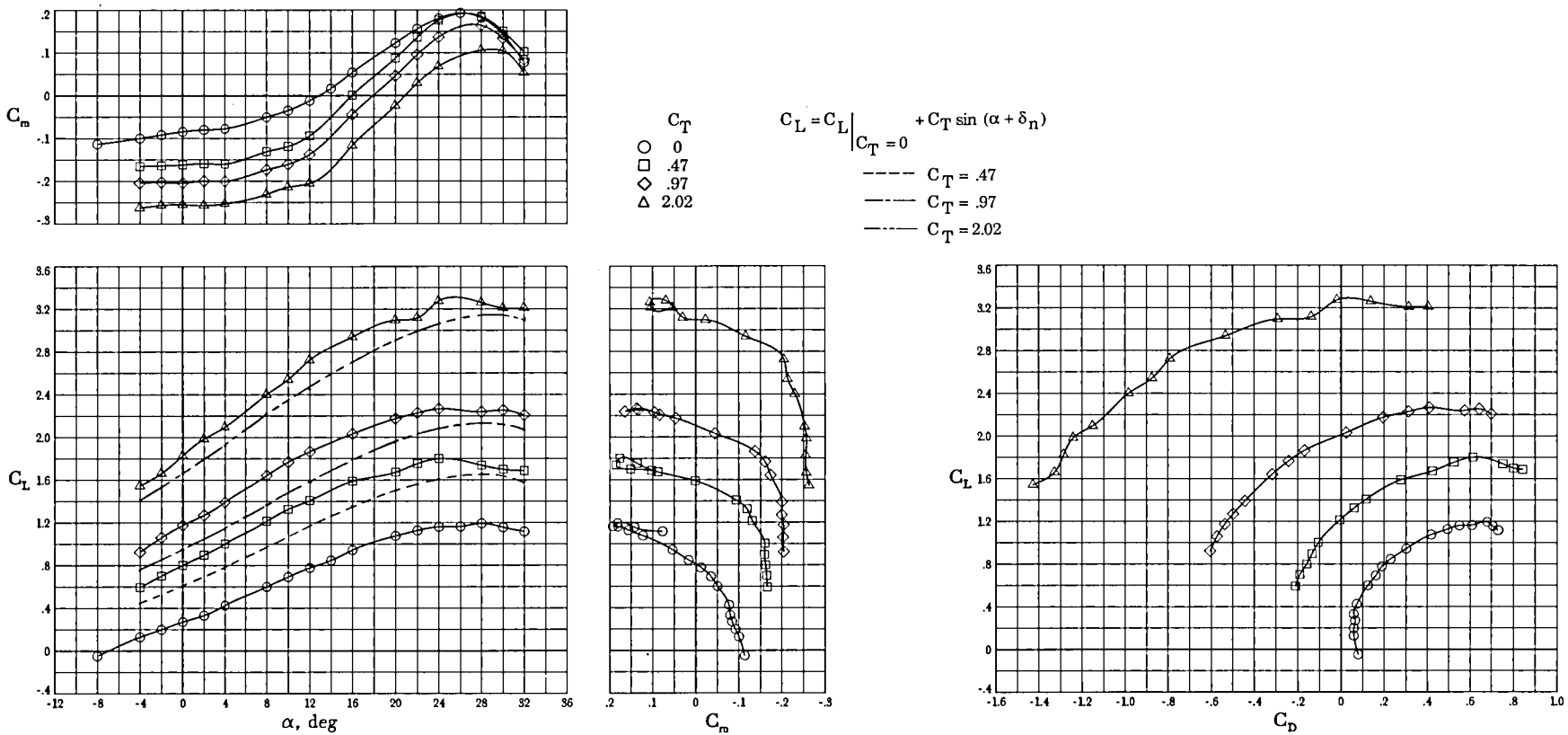

(a) Horizontal tail off.

Figure 11. Effect of thrust on longitudinal aerodynamic characteristics for c.g. at $0.25\bar{c}$. $\delta_{L_1} = 0°$; $\delta_{L_2} = 0°$; $\delta_f = 20°$; $\delta_n = 42.15°$.

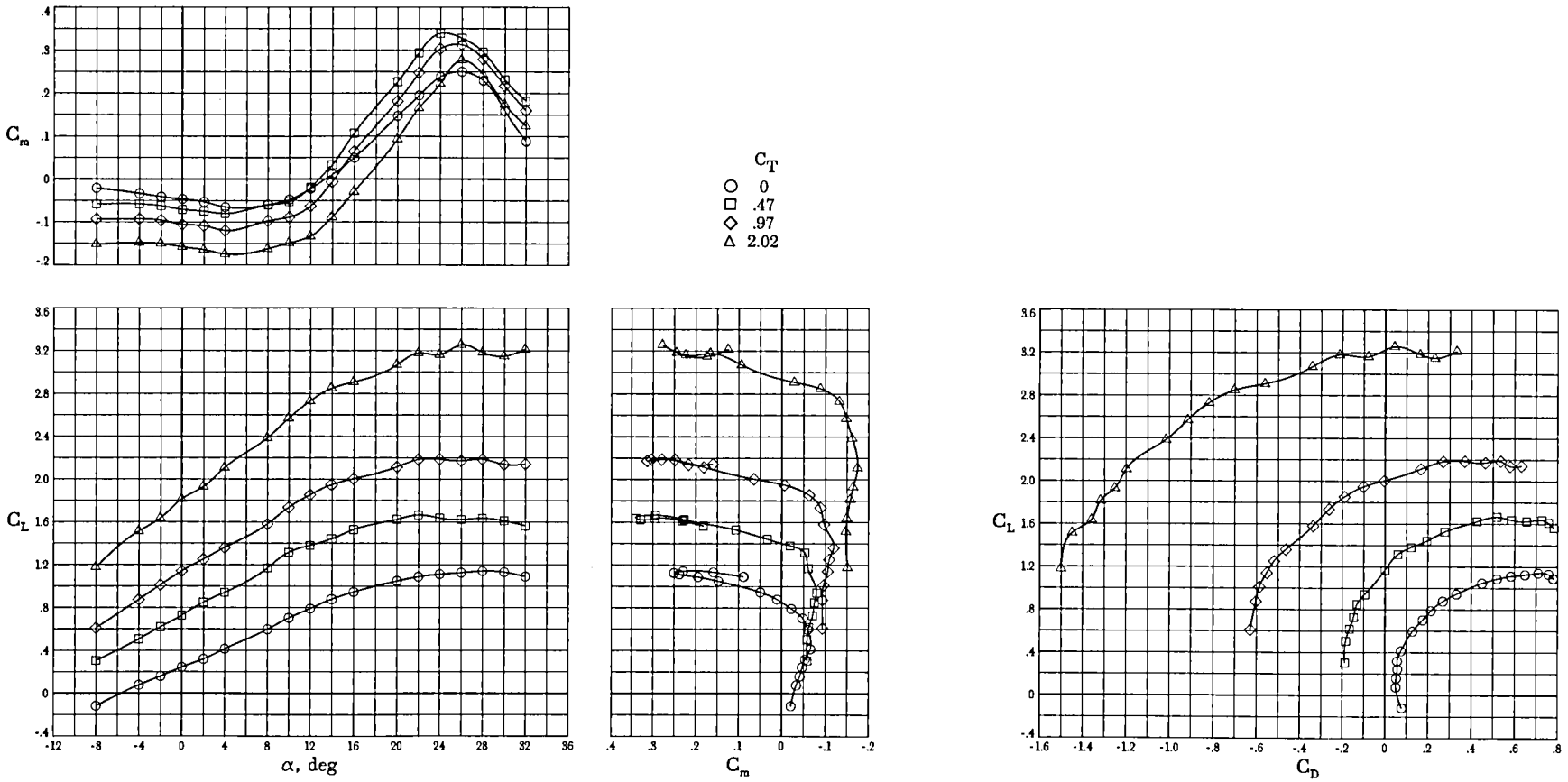

(b) Horizontal tail on; $\delta_e = 0°$.

Figure 11. Concluded.

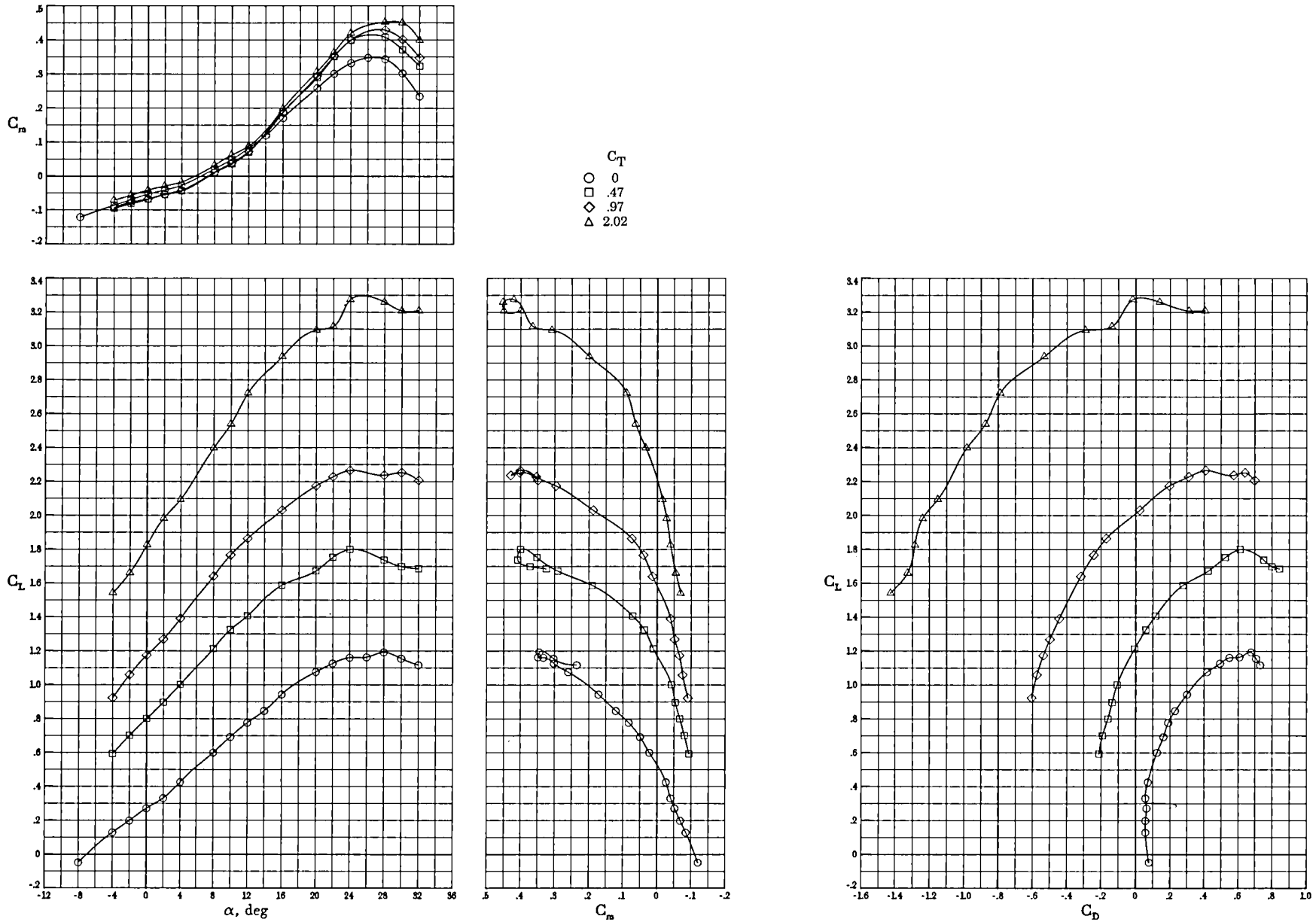

(a) Horizontal tail off.

Figure 12. Effect of thrust on longitudinal aerodynamic characteristics for c.g. at $0.368\bar{c}$. $\delta_{L_1} = 0°$; $\delta_{L_2} = 0°$; $\delta_f = 20°$; $\delta_n = 42.15°$.

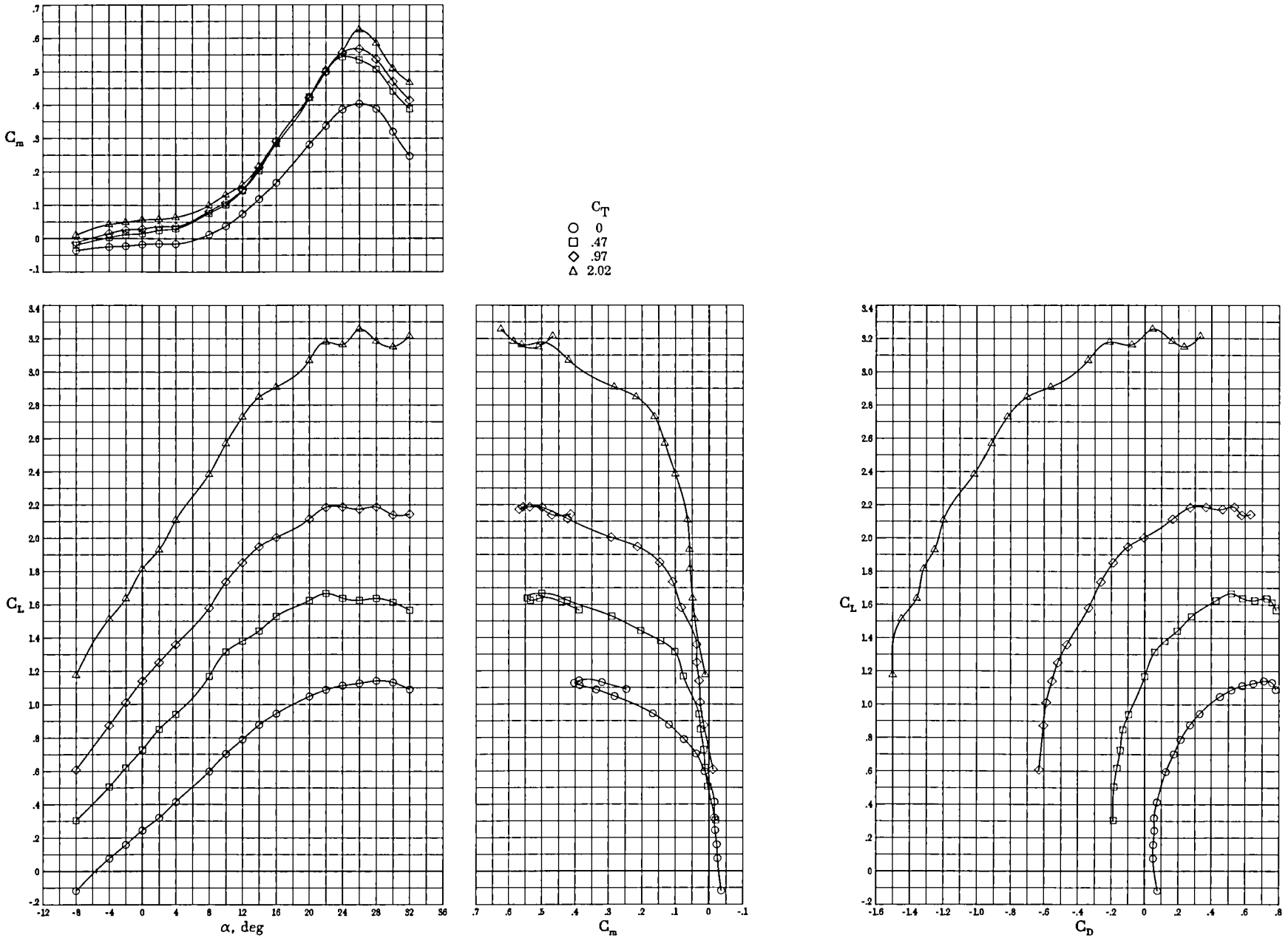

(b) Horizontal tail on.

Figure 12. Concluded.

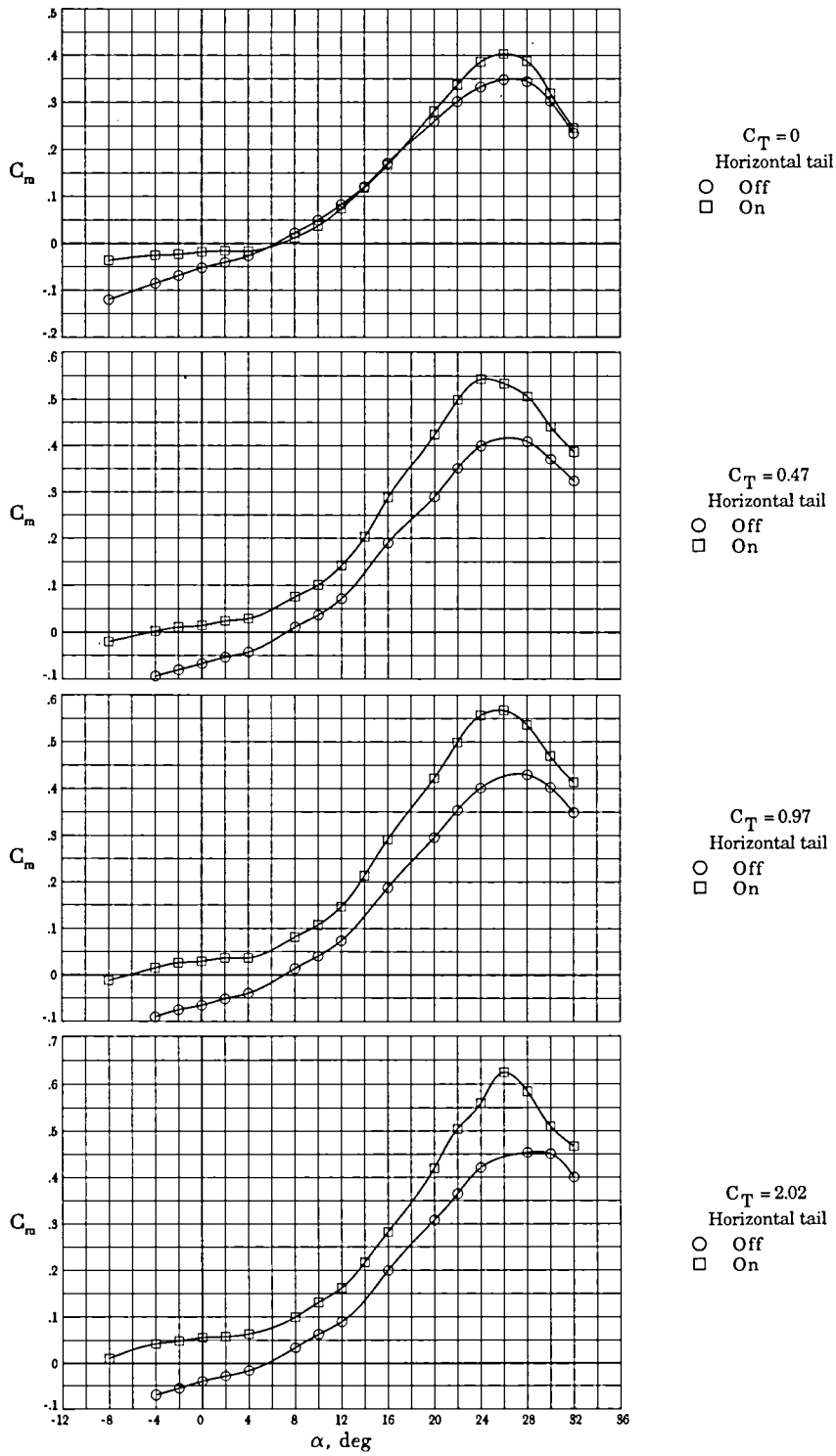

Figure 13. Effect of thrust on horizontal-tail contribution to C_m with $\delta_n = 42.15°$. $\delta_{L_1} = 0°$; $\delta_{L_2} = 0°$; $\delta_f = 20°$; c.g. at $0.368\bar{c}$.

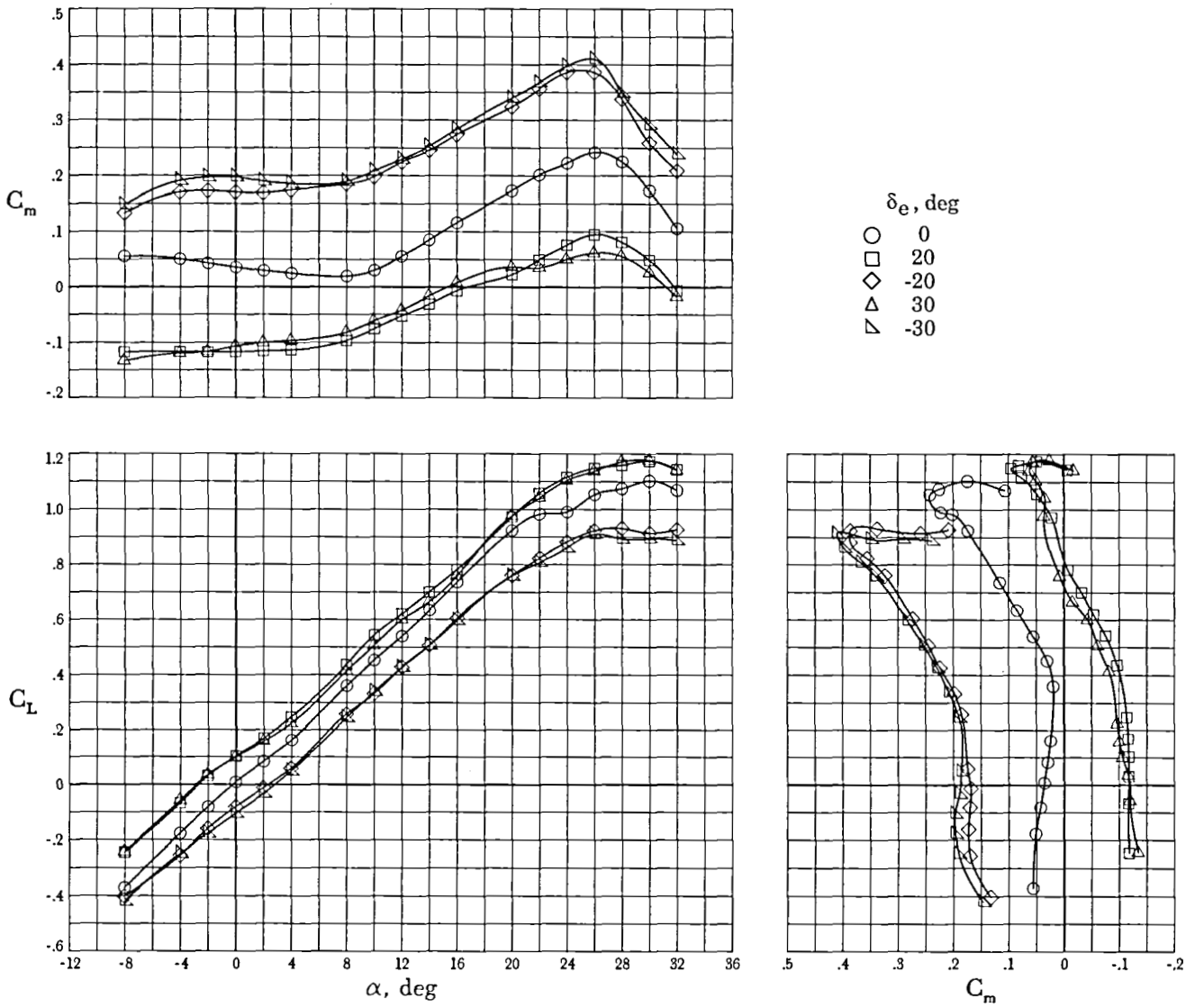

(a) $C_T = 0$.

Figure 14. Elevator effectiveness with $\delta_f = 0°$ and $\delta_n = 0°$. $\delta_{L_1} = 0°$; $\delta_{L_2} = 0°$; c.g. at $0.25\bar{c}$.

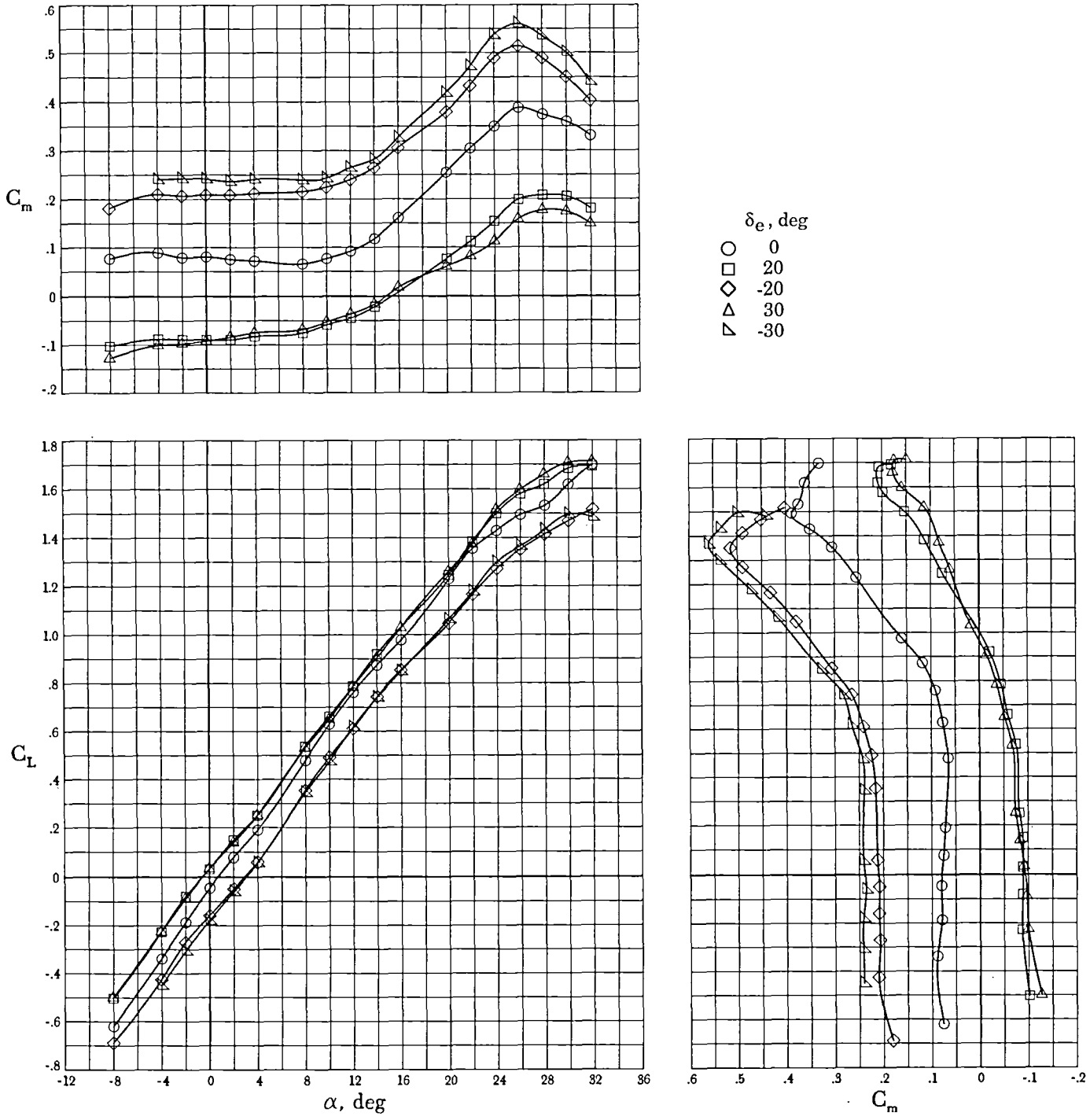

(b) $C_T = 0.90$.

Figure 14. Concluded.

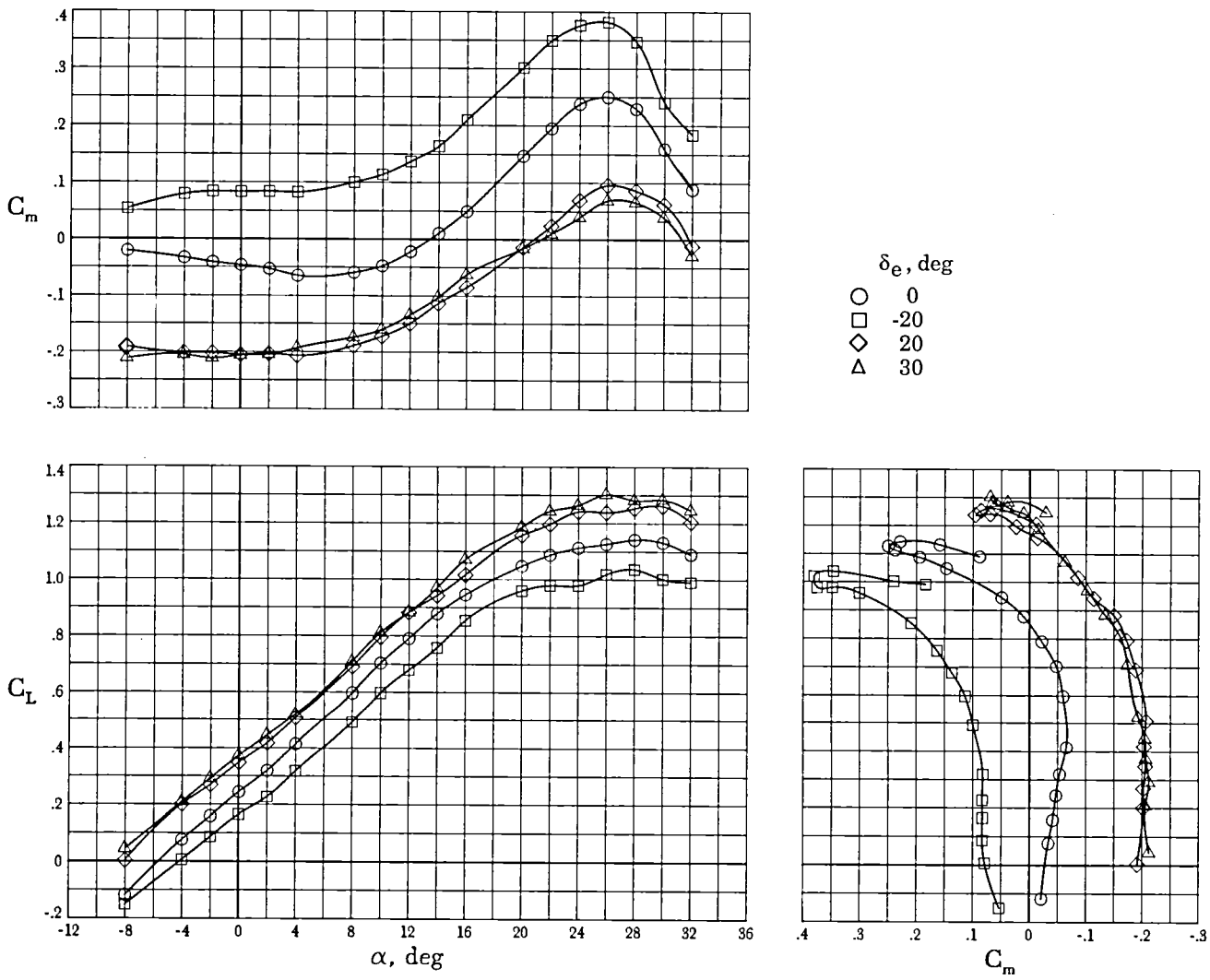

(a) $C_T = 0$.

Figure 15. Elevator effectiveness with $\delta_f = 20°$ and $\delta_n = 42.15°$. $\delta_{L_1} = 0°$; $\delta_{L_2} = 0°$; c.g. at $0.25\bar{c}$.

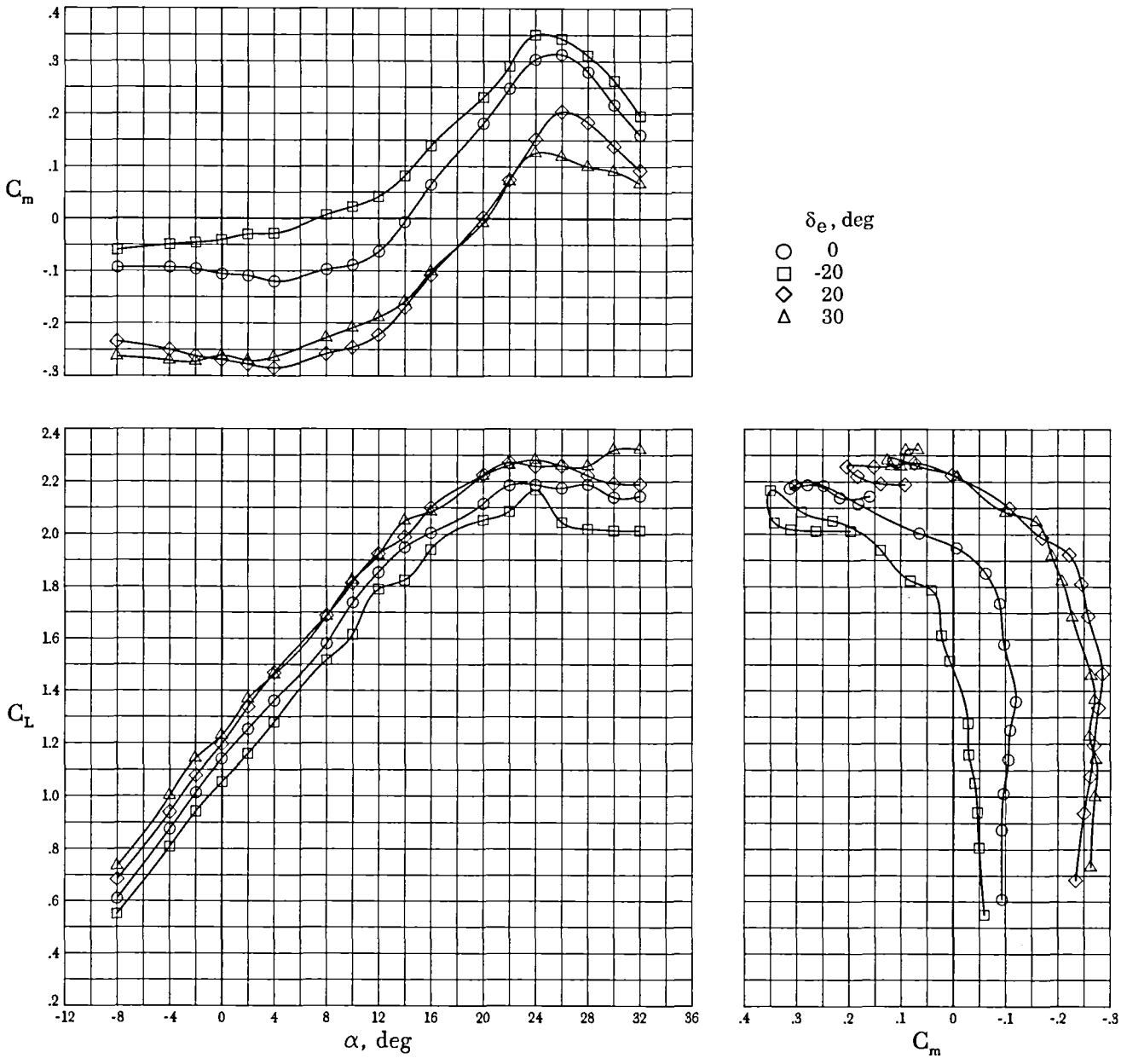

(b) $C_T = 0.97$.

Figure 15. Continued.

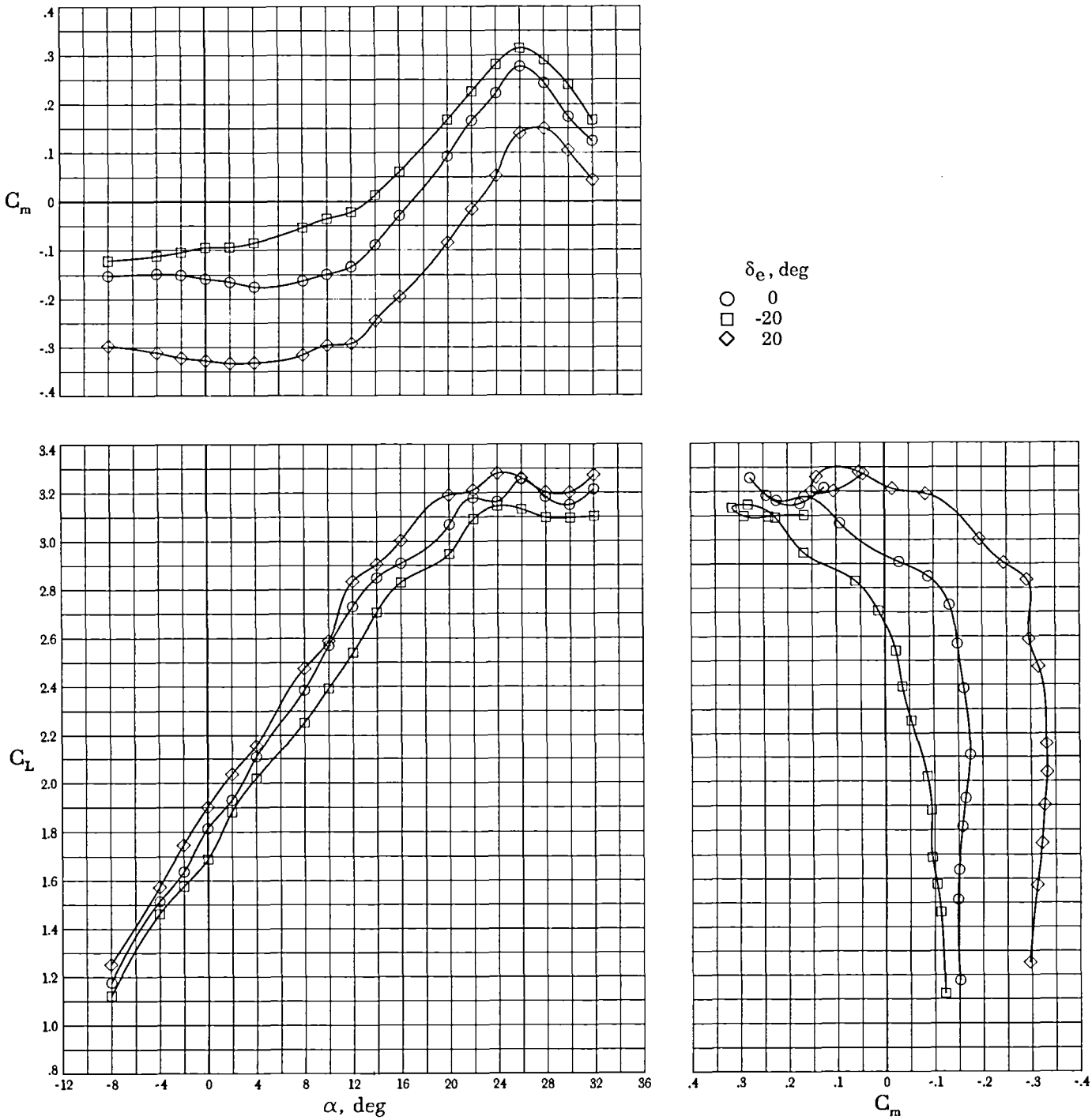

(c) $C_T = 2.02$.

Figure 15. Concluded.

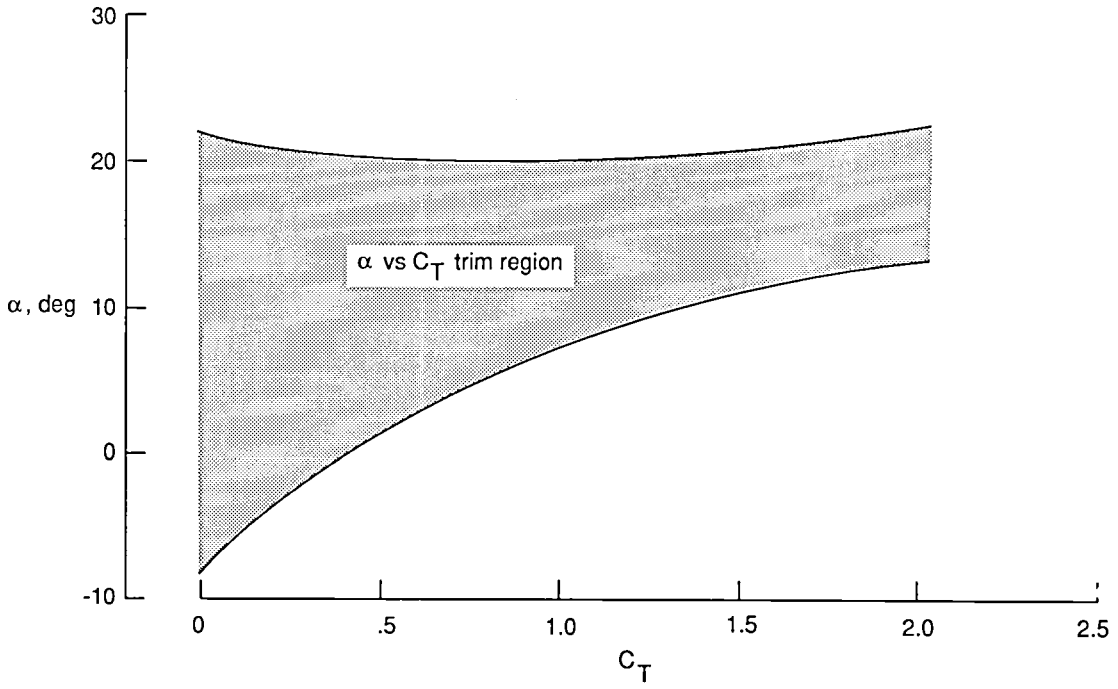

(a) α vs C_T.

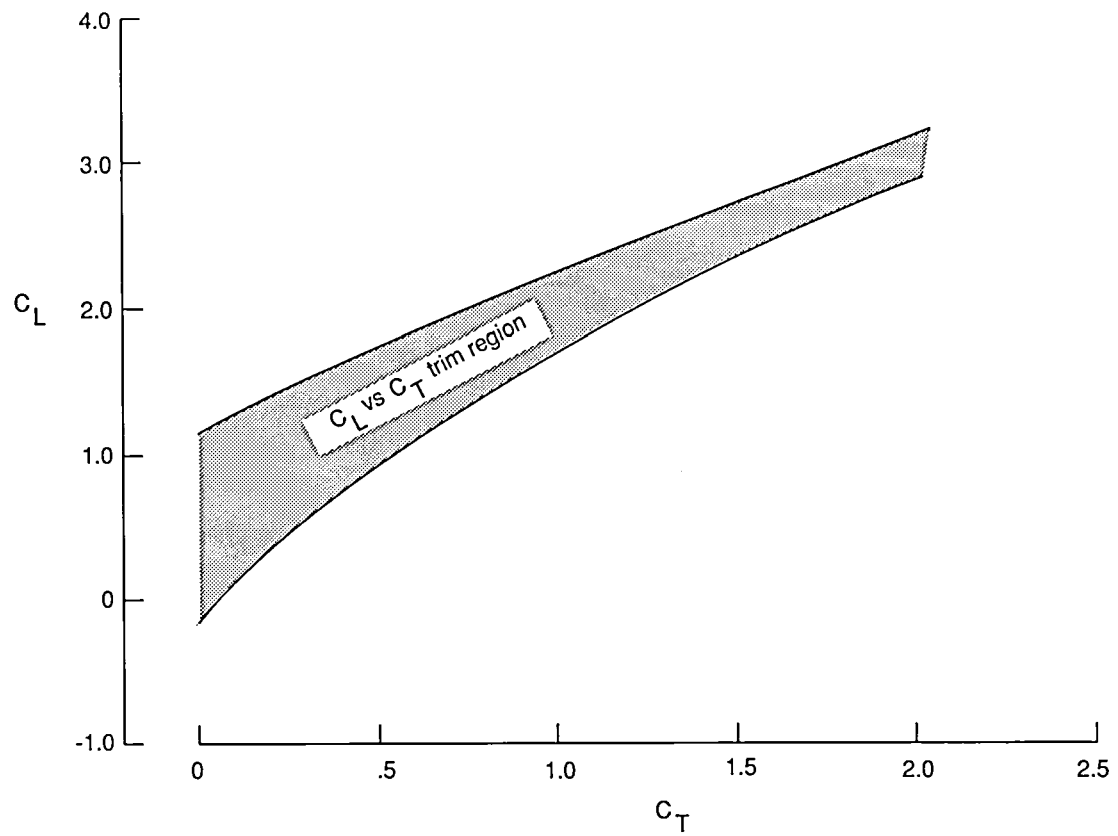

(b) C_L vs C_T.

Figure 16. Trim region for configuration with $\delta_{L_1} = 0°$ and $\delta_{L_2} = 0°$. $\delta_f = 20°$; $\delta_n = 42.15°$; c.g. at $0.25\bar{c}$.

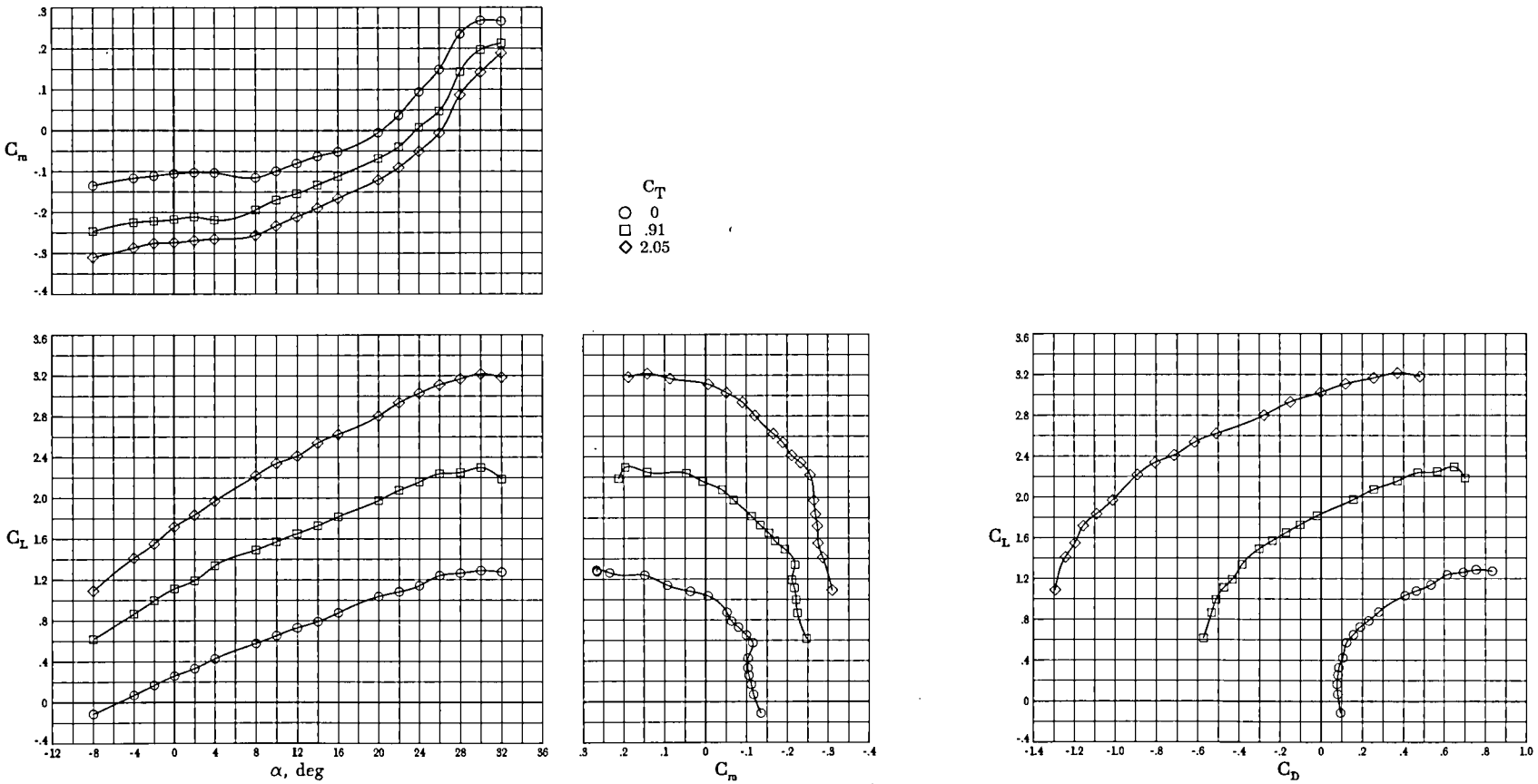

(a) Horizontal tail off.

Figure 17. Effect of thrust on longitudinal aerodynamic characteristics with $\delta_{L_2} = 20°$ for c.g. at $0.25\bar{c}$. $\delta_{L_1} = 0°$; $\delta_f = 20°$; $\delta_n = 42.15°$.

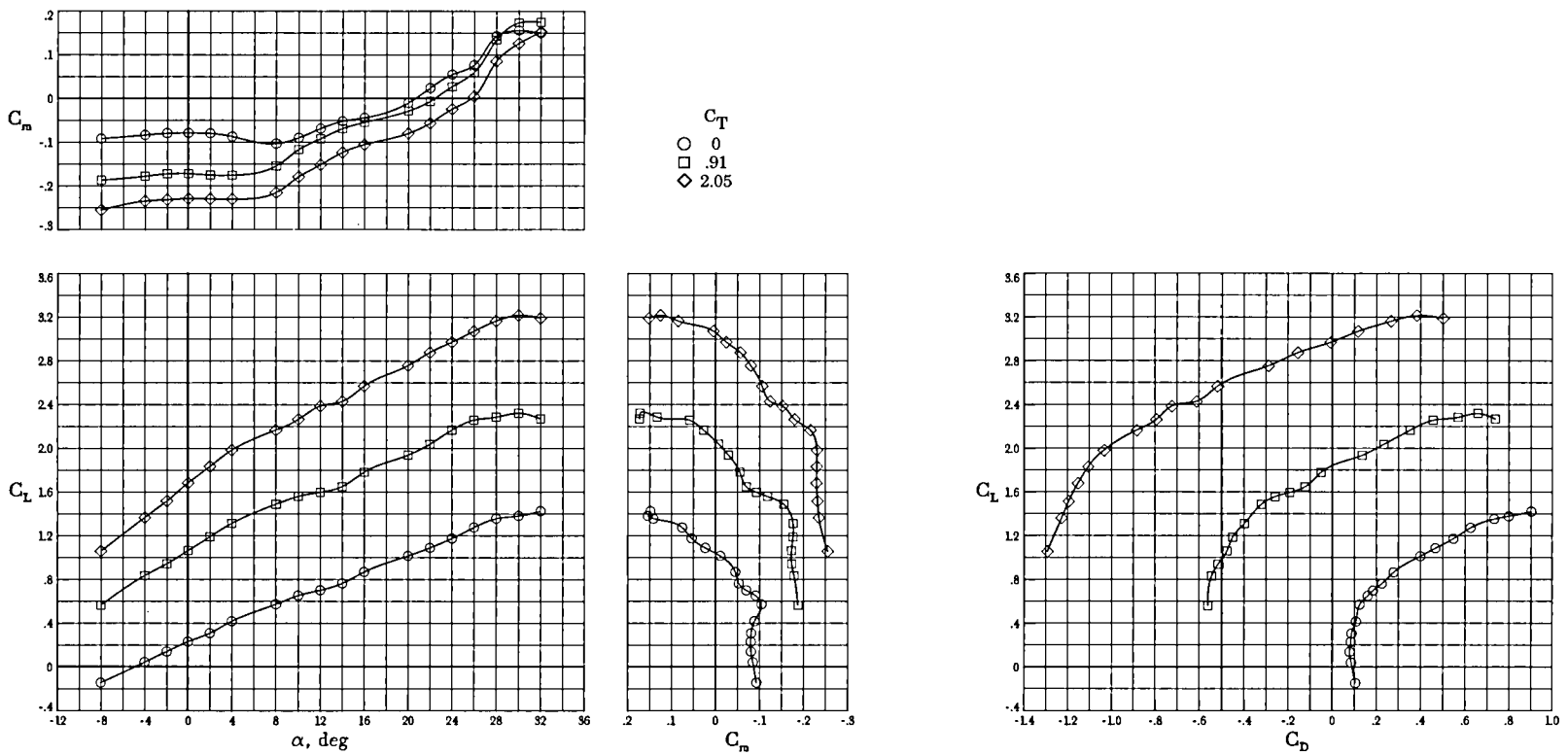

(b) Revised outboard horizontal tail on.

Figure 17. Concluded.

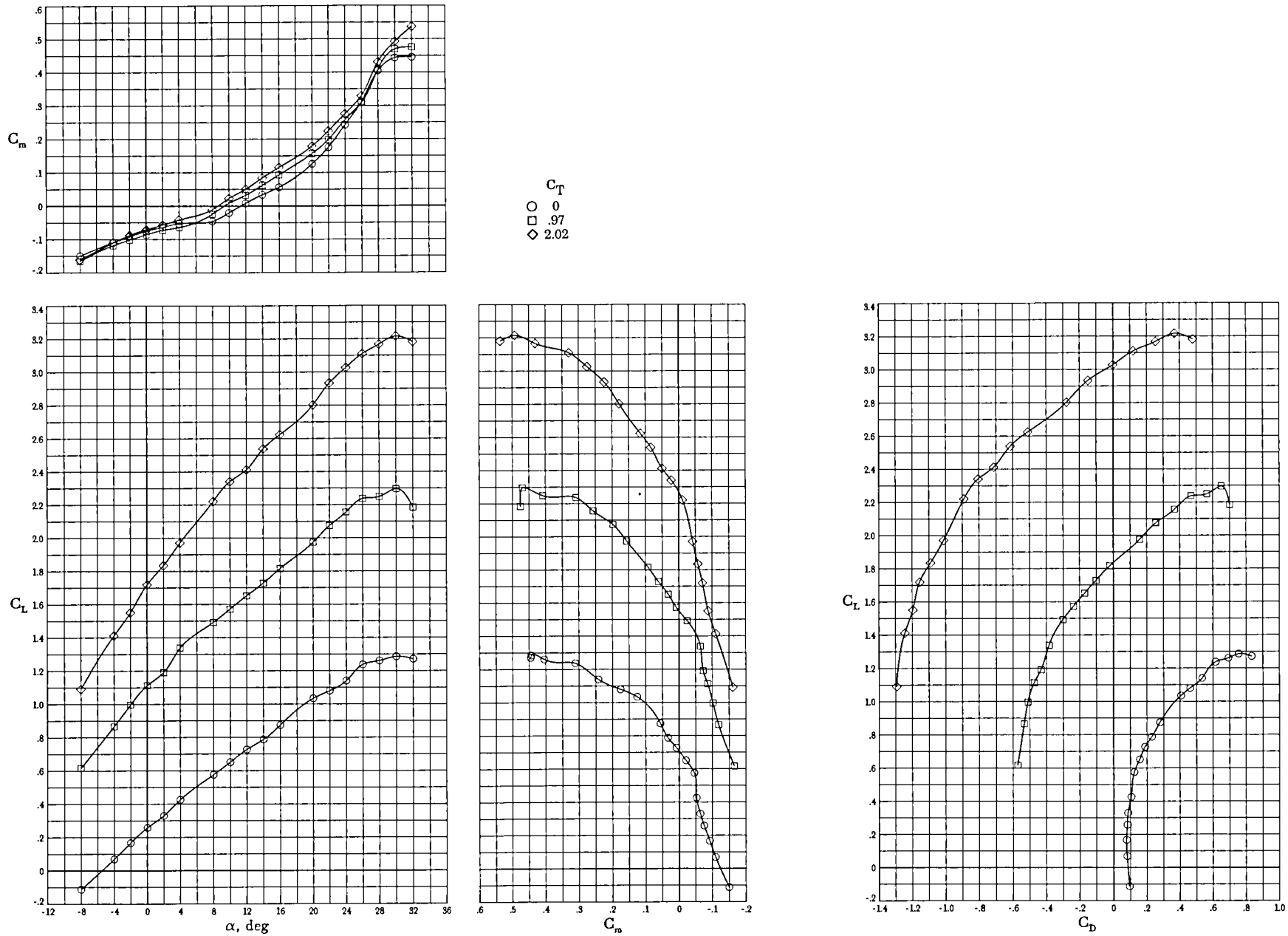

(a) Horizontal tail off.

Figure 18. Effect of thrust on longitudinal aerodynamic characteristics with $\delta_{L_2} = 20°$ for c.g. at $0.368\bar{c}$. $\delta_{L_1} = 0°$; $\delta_f = 20°$; $\delta_n = 42.15°$.

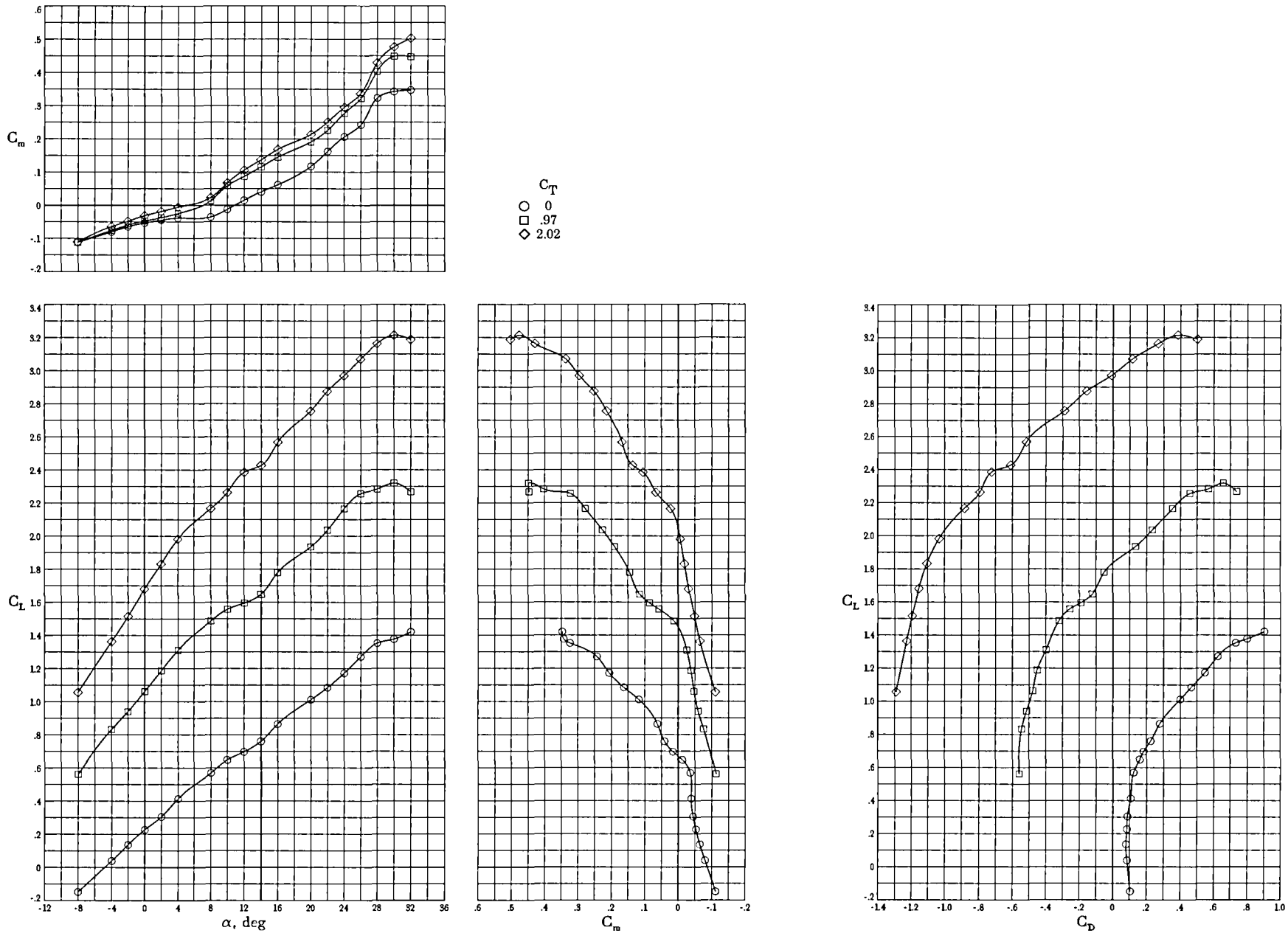

(b) Revised outboard horizontal tail on.

Figure 18. Concluded.

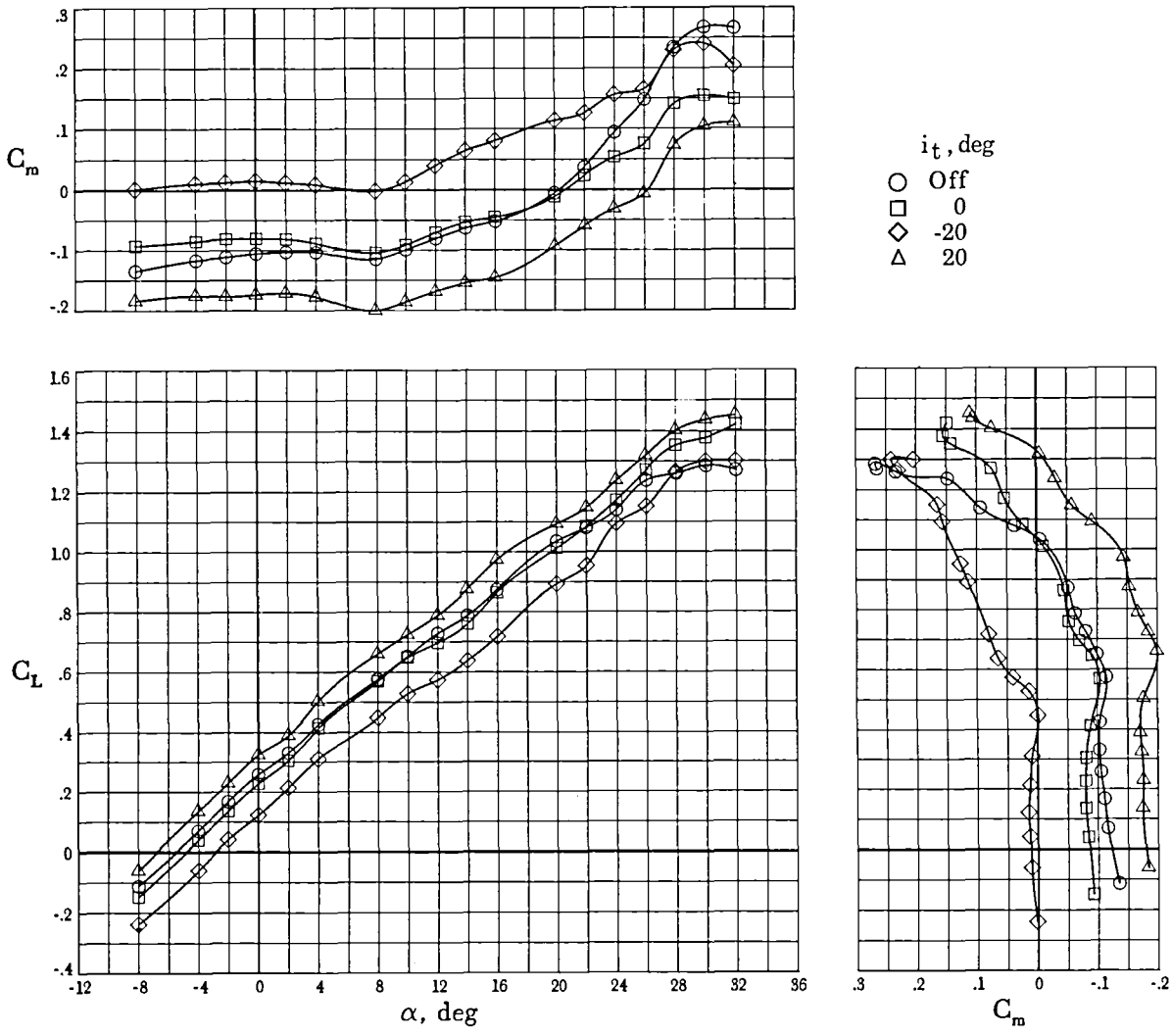

(a) $C_T = 0$.

Figure 19. Effectiveness of revised outboard horizontal tail. c.g. at $0.25\bar{c}$; $\delta_{L_1} = 0°$; $\delta_{L_2} = 20°$; $\delta_f = 20°$; $\delta_n = 42.15°$.

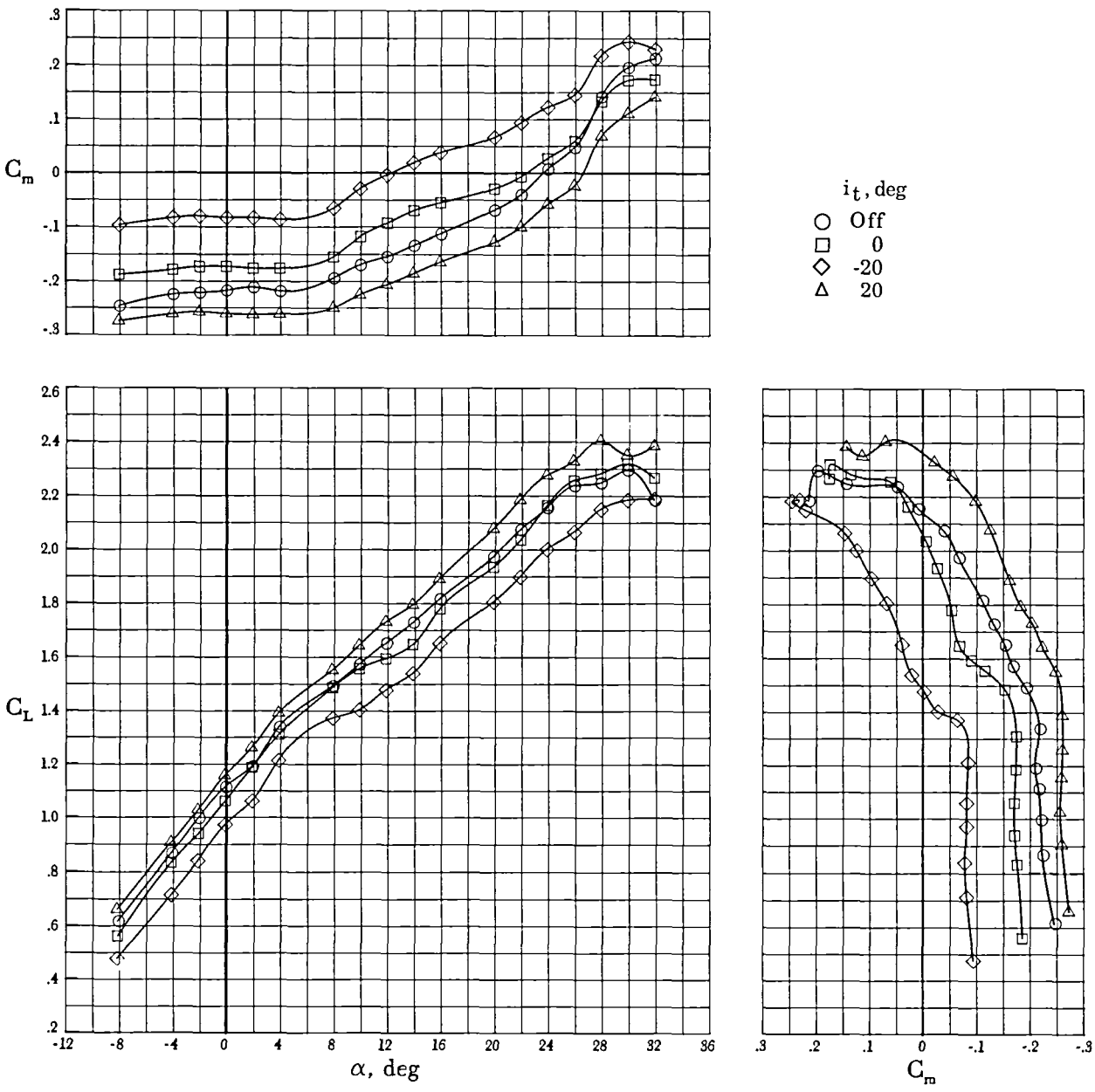

(b) $C_T = 0.97$.

Figure 19. Continued.

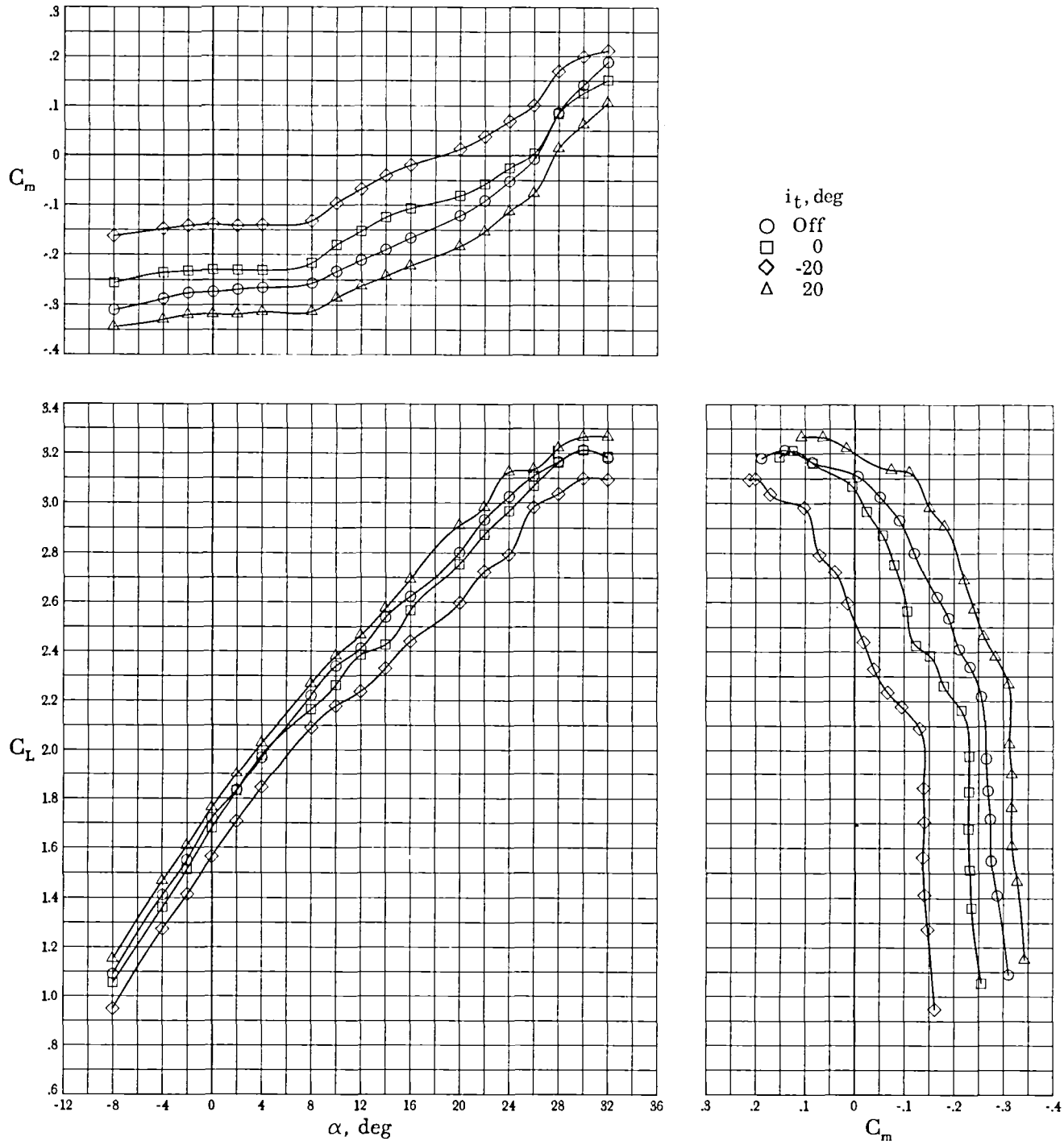

(c) $C_T = 2.02$.

Figure 19. Concluded.

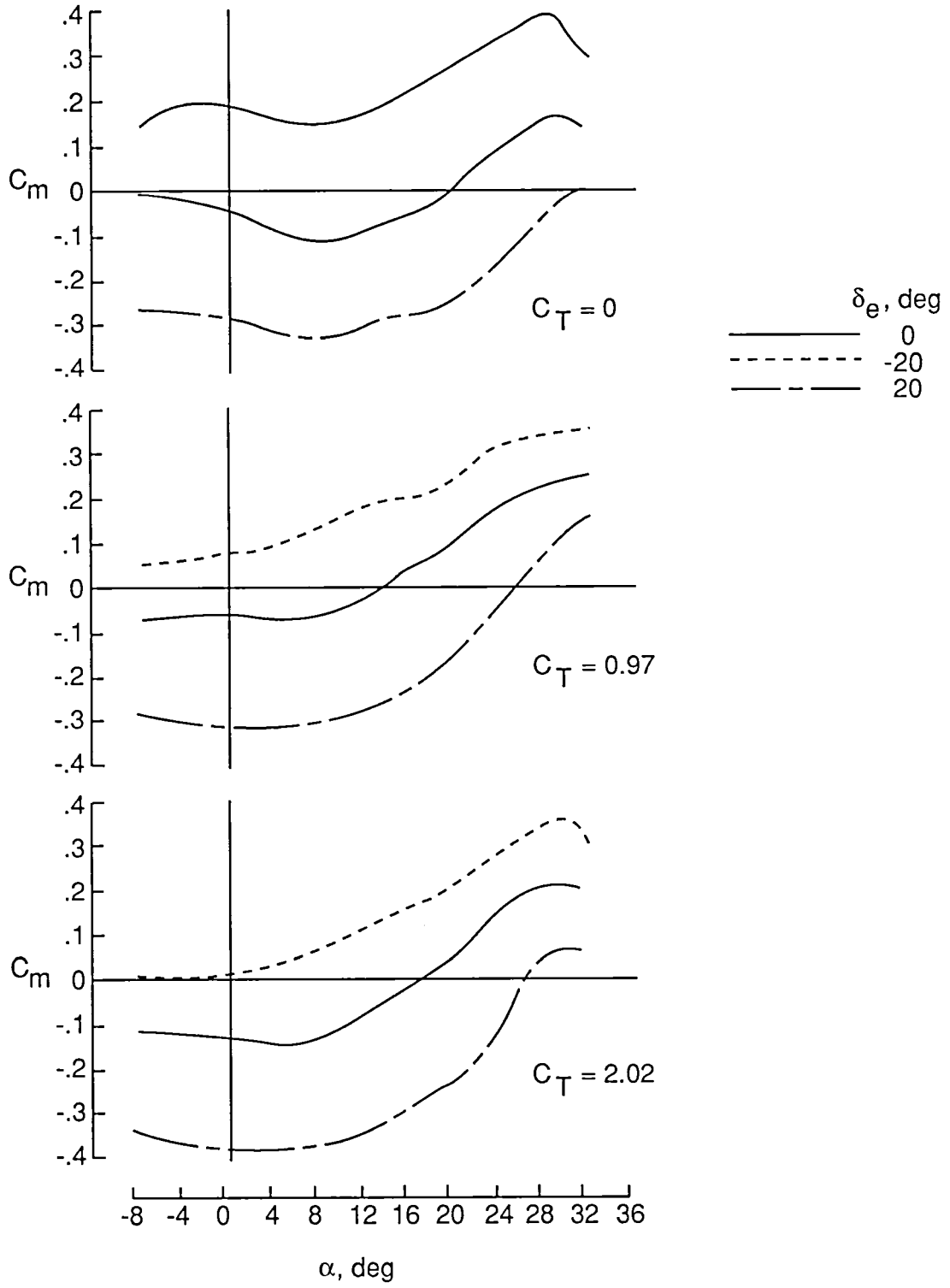

Figure 20. Calculated control effectiveness for high center (baseline) horizontal tail in combination with revised outboard horizontal tail (data of fig. 15 linearly added to data of fig. 19). $\delta_{L_1} = 0°$; $\delta_{L_2} = 20°$; $\delta_n = 42.15°$; $\delta_f = 20°$.

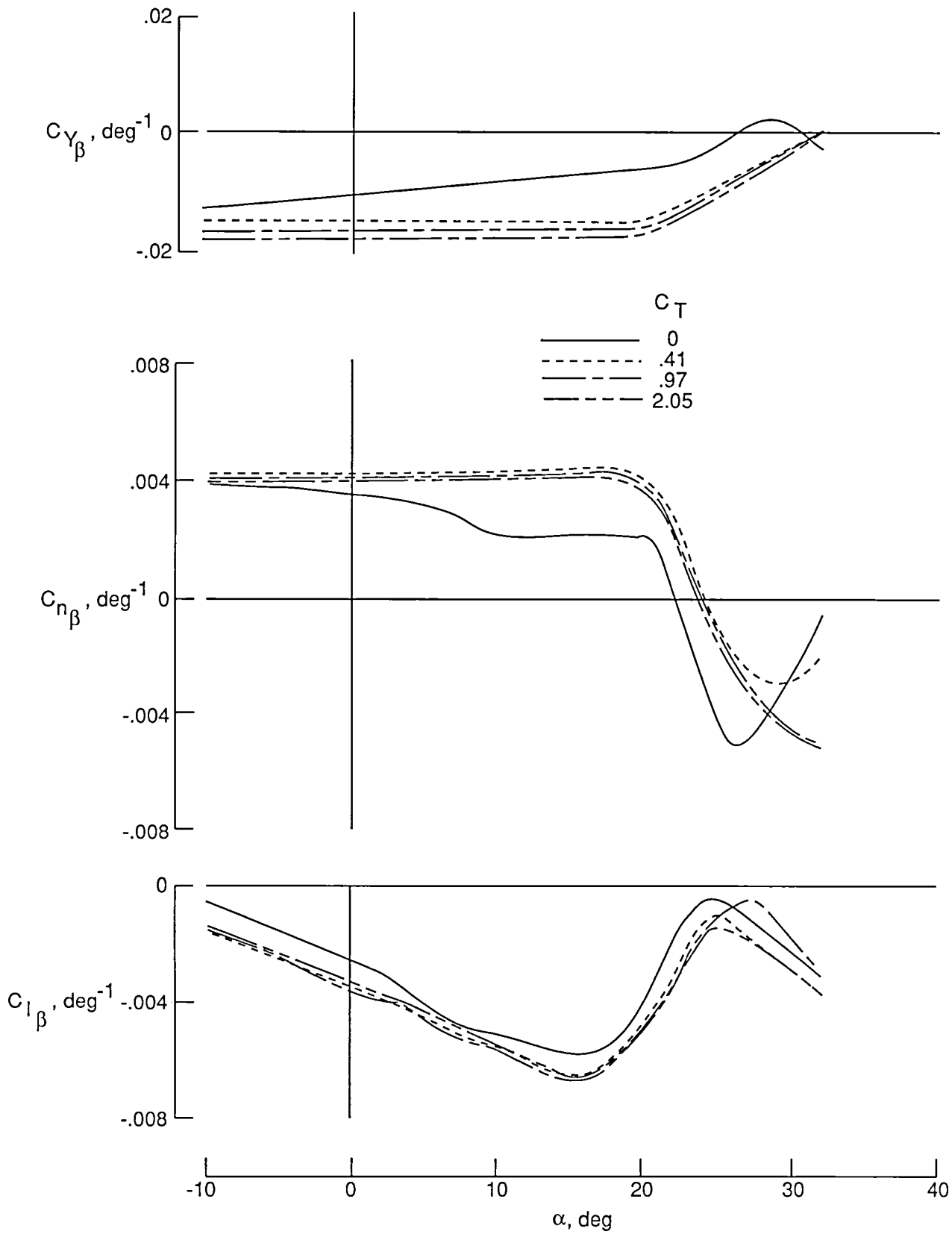

Figure 21. Lateral-directional stability derivatives versus angle of attack. Complete configuration; $\delta_{L_1} = 0°$; $\delta_{L_2} = 0°$; $\delta_f = 20°$; $\delta_n = 42.15°$.

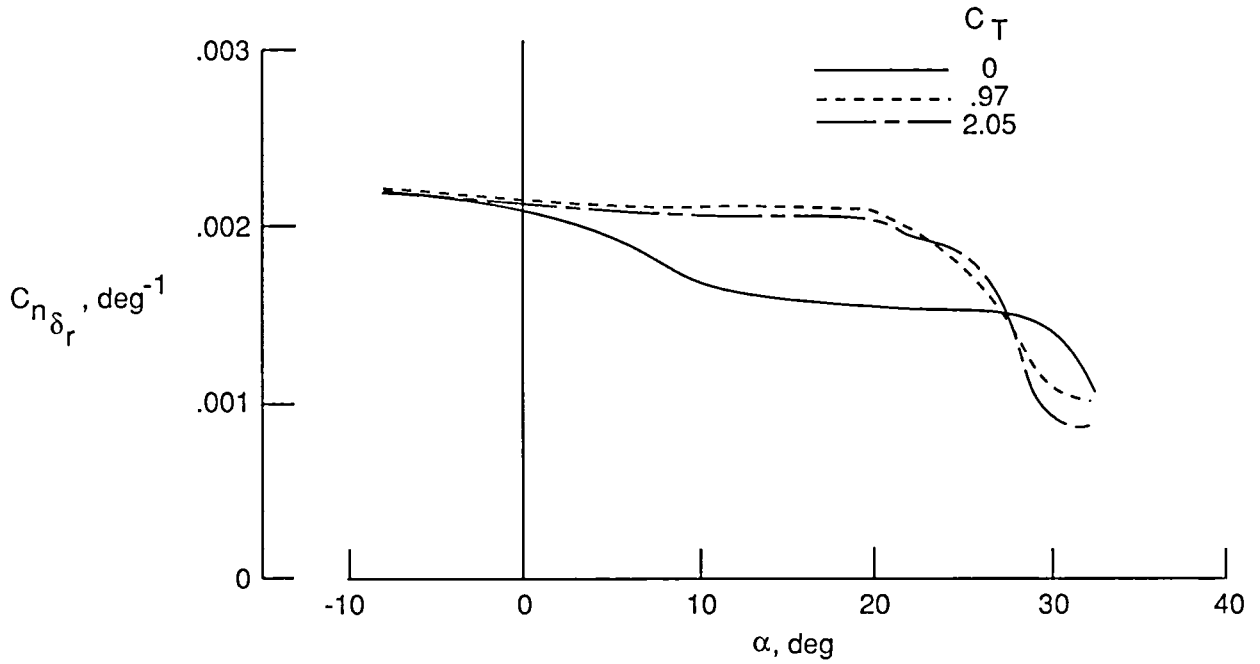

Figure 22. Rudder effectiveness for complete configuration. $\delta_{L_1} = 0°$; $\delta_{L_2} = 0°$; $\delta_f = 20°$; $\delta_n = 42.15°$; c.g. at $0.25\bar{c}$.

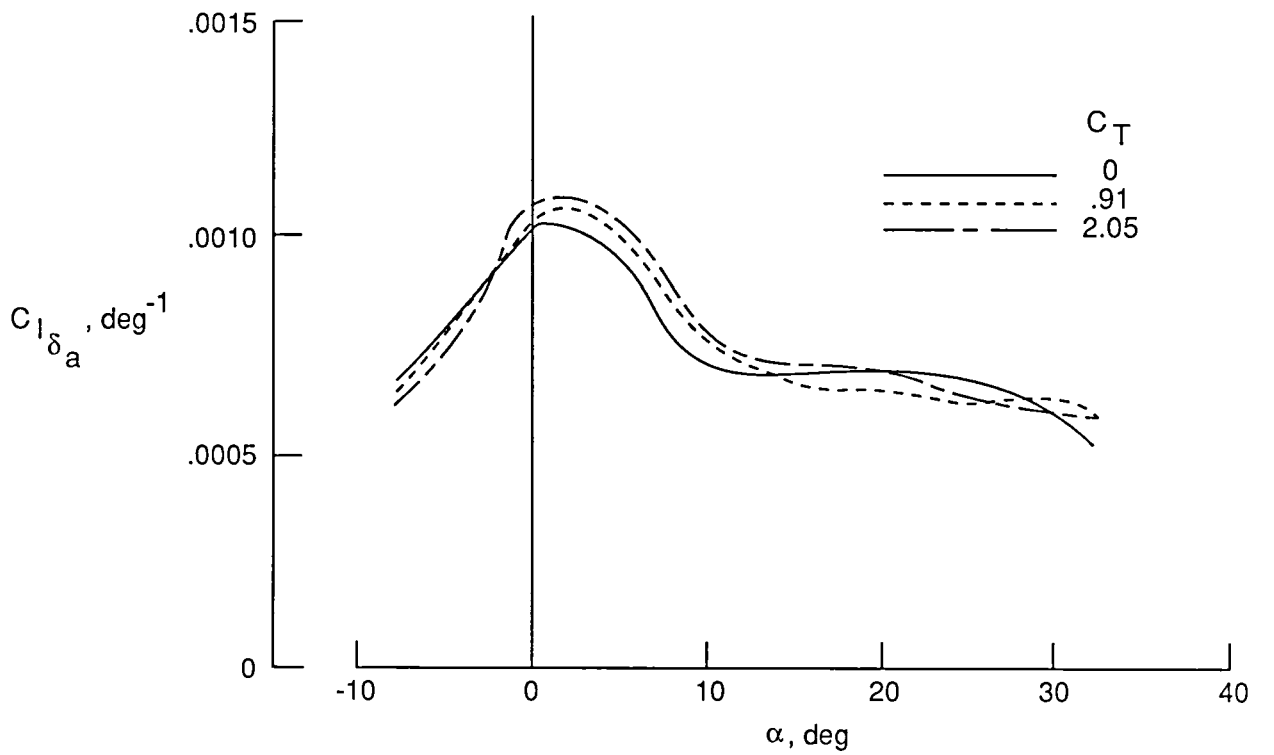

Figure 23. Aileron effectiveness for complete configuration. $\delta_{L_1} = 0°$; $\delta_{L_2} = 0°$; $\delta_f = 20°$; $\delta_n = 42.15°$; c.g. at $0.25\bar{c}$.

NASA
National Aeronautics and Space Administration

Report Documentation Page

1. Report No.	2. Government Accession No.	3. Recipient's Catalog No.
NASA TM-4050		

4. Title and Subtitle	5. Report Date
Low-Speed Wind-Tunnel Test of a STOL Supersonic-Cruise Fighter Concept	July 1988
	6. Performing Organization Code
7. Author(s)	8. Performing Organization Report No.
Paul L. Coe, Jr., and Donald R. Riley	L-16422
	10. Work Unit No.
9. Performing Organization Name and Address	505-61-71-07
NASA Langley Research Center Hampton, VA 23665-5225	11. Contract or Grant No.
	13. Type of Report and Period Covered
12. Sponsoring Agency Name and Address	Technical Memorandum
National Aeronautics and Space Administration Washington, DC 20546-0001	14. Sponsoring Agency Code

15. Supplementary Notes

16. Abstract

A wind-tunnel investigation was conducted to examine the low-speed static stability and control characteristics of a 0.10-scale model of a STOL fighter concept capable of efficient long-range supersonic cruise. The configuration has long twin booms extending aft of the engine to the twin vertical tails, which support a high center horizontal tail. The propulsion system features a two-dimensional thrust-vectoring exhaust nozzle which is located so that the nozzle hinge line is near the aircraft center of gravity. This arrangement is intended to allow large thrust-vector angles to be used to obtain significant values of powered lift while pitching-moment trim changes are minimized. The investigation obtained low-speed stability and control information over an angle-of-attack range including the stall. The investigation also included a study of jet-induced power effects.

17. Key Words (Suggested by Authors(s))

STOL
Supersonic cruise
Vectored thrust

18. Distribution Statement

Unclassified—Unlimited

Subject Category 08

19. Security Classif.(of this report)	20. Security Classif.(of this page)	21. No. of Pages	22. Price
Unclassified	Unclassified	42	A03

National Aeronautics and
Space Administration
Code NTT-4

Washington, D.C.
20546-0001